Alma Mater Studiorum - Università di Bologna

SCUOLA DI SCIENZE

Dipartimento di Chimica Industriale"Toso Montanari"

Corso di Laurea Magistrale in

Chimica Industriale

Classe LM-71 - Scienze e Tecnologie della Chimica Industriale

Atropisomeric Xanthines: Synthesis, Stereodynamics And Absolute Configuration

Tesi di laurea sperimentale

CANDIDATO

Sofia Perticarari

RELATORE

Prof. Dr. Andrea Mazzanti

CORRELATORE

Dr. Michele Mancinelli

Sessione I
_____
Anno Accademico 2014-2015
_____

Abstract

During the thesis period a new class of atropisomeric xanthine derivatives has been studied. We decided to focus our attention on these purine bases because of their various biological activities, that could play an important role in the discovery of new bioactive atropisomers. The synthesized compounds bear an Aryl-N chiral axis in position 1 of the xanthine scaffold, around which the rotation is prevented by the presence of bulky *ortho* substituents. Through a retro synthetic analysis we synthesized three atropisomeric structures bearing in position 1 of the purine scaffold respectively an *o*-tolyl, *o*-nitrophenyl and a 1-naphthyl group. The conformational studies by DFT simulations showed that the interconversion energy barrier between the two available skewed conformations is higher enough to obtain thermally stable atropisomers. After the separation of the atropisomers, the experimental energy of interconversion was investigated by means of kinetic studies following the thermal racemization process using an enantioselective HPLC column. The absolute configuration of each atropisomer was assigned by experimental ECD analysis and TD-DFT simulations of the ECD spectra.

Durante il periodo di tesi, è stata studiata una nuova classe di derivati xantinici atropisomerici. Abbiamo deciso di rivolgere la nostra attenzione verso queste basi puriniche, a causa delle loro note attività biologiche, tali da poter svolgere un ruolo importante nella produzione di nuovi composti atropisomerici farmacologicamente attivi. Le strutture sintetizzate non appartengono alla classe dei sistemi biarilici, bensì sono caratterizzate da un asse chirale arile-N in posizione 1 dello scheletro xantinico. La rotazione attorno a tale asse è impedita dalla presenza di gruppi arilici *orto* sostituiti. A seguito di un'analisi retro sintetica, sono state sintetizzate tre strutture atropisomeriche recanti rispettivamente un *o*-tolile, un *o*-nitro-fenile e un gruppo naftile. Gli studi conformazionali effettuati con simulazioni DFT hanno dimostrato che la barriera energetica di interconversione tra le due conformazioni enantiomeriche è abbastanza alta da poter ottenere atropisomeri stabili a temperatura ambiente. Separati gli atropisomeri è stata studiata l' energia sperimentale di interconversione mediante analisi cinetiche, monitorando il processo di racemizzazione termica con l'ausilio di una colonna HPLC enantioselettiva. La configurazione assoluta di ogni atropisomero è stata assegnata tramite simulazioni TD-DFT degli spettri ECD, comparati con gli sperimentali.

Index

1. Introduction

1.1 Axial chirality and atropisomerism

"The universe is asymmetric and I am persuaded that life, as it is known to us, is a direct result of the asymmetry of the universe or of its indirect consequences." (Louis Pasteur, *L'univers est dissymetrique).*

In 1848, Louis Pasteur recognized the omnipresence and significance of chirality. He realized that chiral objects exist as a pair of enantiomorphous mirror images that are non-superimposable and related to each other, as stated also by Lord Kelvin in 1884, when he affirmed *"I call any geometrical figure, or group of points, chiral, and say that it has chirality, if its image in a plane mirror, ideally realized, cannot be brought to coincide with itself".*

Today, we know that chirality can be encountered at all levels in nature; it is a key feature of natural compounds and plays an essential role in amino acids, peptides and proteins, sugars and numerous bioactive substances, including most of the drugs that are used in medicine.

At the molecular level, chirality gives rise to enantiomers that can exhibit different chemical, physical and biological properties in a chiral environment.

Stereochemistry embraces a broad variety of closely intertwined static and dynamic aspects that are all related to the three-dimensional structure of molecules. While static stereochemistry deals with the spatial arrangement of atoms in molecules, dynamic stereochemistry emphasizes structural change and comprises asymmetric reactions as well as interconversion of configurational and conformational isomers. The stereodynamic chemistry plays a fundamental role in modern chemistry, from asymmetric synthesis and drug discovery to material sciences.[1]

Axial chirality is referred to molecules that do not possess a classic stereogenic center, but one or more stereogenic axes about which a set of substituents is held in a spatial arrangement that is not superimposable on its mirror image. So the presence of axial chirality generates different conformers that may be stable at ambient temperature, depending on the rotational energy barrier required for racemization of the chiral axis.

Bringmann further affirmed the preconditions for axial chirality in his review[2], adding that three major factors governing the minimum free energy barrier to rotation: (1) the combined steric demands of substituents close to the axis; (2) the length and rigidity of bridges (if present); and (3) the mechanisms involved in isomerization.

This source of chirality is called "atropisomerism" (from the Greek, α meaning *not* and $\tau\rho\sigma\pi\sigma\sigma$ meaning *turn*), a term proposed by Kuhn in 1933[3] to describe molecules with a chiral axis maintained by hindered rotation about a single bond. This restricted rotation sees the origin of compounds with conformational chirality that have enantiomers that can interconvert without breaking any covalent bonds, called atropisomers.[4]

So, atropisomers are a subclass of conformers that result from slow rotation around a single bond due to steric hindrance and/or electronic factors.

Before the rationalization by Kuhn, atropisomerism was first detected in 6,6'-dinitro-2,2'-diphenic acid, the enantiomers of which were successfully resolved by Christie and Kenner[5] in 1922.

In 1983, Oki proposed a boundary between atropisomers and conformers (and therefore between configuration and conformation) with his arbitrary definition that atropisomers are conformers which interconvert with a half-life $t_{1/2}$ of at least 1000 s (16.7 min) at +25 °C, corresponding to a racemization barrier of 21.8 kcal/mol.[6]

Given the absence of a standard stereogenic centre, the absolute configuration of these molecules has to be related to the dihedral angle generated by the chiral axis.
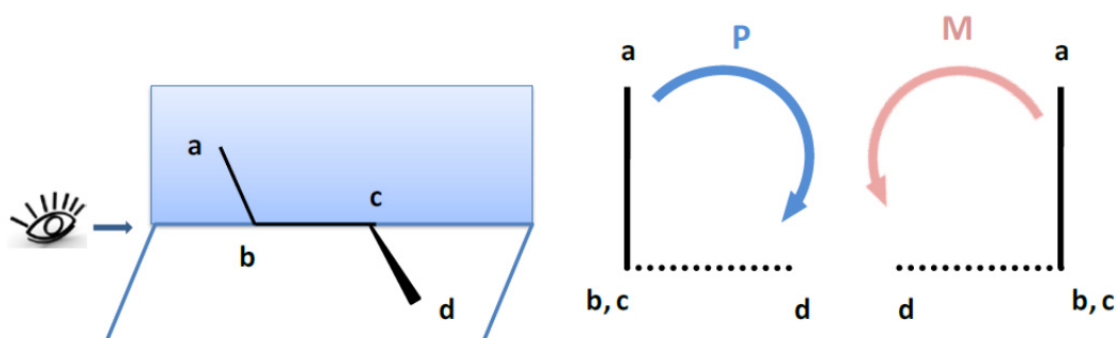

Figure 1 Schematic representation of a dihedral angle and its nomenclature.

In a chain of atoms **a-b-c-d** (Figure 1), the torsion angle is the dihedral between the plane containing the atoms **a**, **b**, **c** and that containing **b**, **c**, **d** (from -180° to +180°) This system has two extreme conformations called *anti* and *eclipsed* (180 and 0°, respectively). The torsion

angle between groups **a** and **d** is then considered to be positive (absolute configuration is *P* or Δ) if the bond **a-b** is rotated in a clockwise direction in order to eclipse the bond **c-d** by moving away from the observator. A negative torsion angle requires rotation in the opposite sense (absolute configuration is *M* or Λ).[7]

The Cahn-Ingold-Prelog priority rules are applied to the substituents bonded to atoms **b** and **c** to find atoms **a** and **d** and allow the sign of the dihedral angle to be assigned. It is important to note that the sign of a dihedral angle remains the same regardless of the side from which it is observed, provided that the observation starts from the nearest atom and follows the chain toward the farthest.

The concept of axial chirality as a stereogenic source in a rotationally hindered compound was for many years relegated to the academic field. However this situation changed with the discovery of many bioactive natural compounds containing stereogenic chiral axes[8] and with the discovery of many catalysts useful for asymmetric synthesis.[2]

The most popular atropisomeric systems used for asymmetric synthesis contain the binaphthyl scaffold, where BINAP[9] is undoubtedly the most famous example (Figure 2). As pioneered by Noyori and his co-workers, Rh complexes of BINAP are useful for the chemoselective hydrogenation of C=C and C=O bonds. For the studies in chirally catalysed hydrogenations Noyori was awarded the Nobel Prize in Chemistry in 2001.
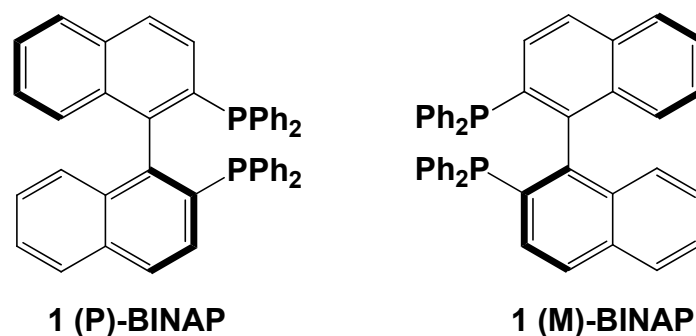

Figure 2 The two enantiomers of BINAP

The search for new atropisomeric systems and the related conformational analysis can be considered nowadays as an open research field.

1.2 Atropisomerism in drug discovery

The goal for drug discovery is to develop safe and stable substances that specifically target essential elements that cause disease. The presence of a source of chirality is an additional contribute to the specificity and complexity of a biologically active compound. The inherent chirality of biological systems often results in vastly different biological effects of enantiomers on the target of interest: classical chiral centre enantiomers have been shown to differ significantly in biological activity, pharmacodynamics, pharmacokinetics and toxicity.[8b] The well-known cases of thalidomide[10] and perhexiline,[11] whose enantiomers led to unexpected effects in humans regarding toxicity and metabolic properties, emphasized the importance of addressing stereochemistry in drug development. Therefore, it is required by regulatory agencies such as the U.S. Food and Drug Administration (FDA) that chiral drugs are developed as single enantiomers in cases when this gives improved safety and/or efficacy.[12] However, there are some drugs for which mixtures of enantiomers have acceptable toxicological profiles; if the mixture is not reasonably separable or if racemization is rapid in vitro and/or in vivo, it would be futile to administer a single enantiomer (for example ibuprofen is sold as a racemic mixture).[13] Overall for racemic drug candidates there must be an acceptable toxicology and pharmacokinetic profile. In pharmaceutical industry stereoisomers are most frequently observed as a result of chiral centers, but atropisomerism can be another, yet overlooked, source of drug chirality.

Anyway the FDA's statements are referred to classical chiral centered molecules, whereas there are no direct guidelines from regulatory agencies on how to deal with atropisomers.

Atropisomerism may give rise to geometrical isomers, diastereoisomers, or enantiomers, all with the feature that they can be thermally equilibrated, involving an intramolecular dynamic process that is bond rotation. Moreover, bond rotation is time-dependent and half-life for atropisomers can vary between minutes to years, depending on the steric hindrance, electronic interactions, temperature and solvent. Because of this time-dependent feature, drug discovery campaigns can become more complex. Recently LaPlante, Edwards and co-workers[8b] gave some guidelines to manage this time-dependent feature in the development of atropisomeric drugs. The authors suggest to compute the torsion rotational energy barriers to predict the existence of atropisomerism along the drug discovery pathway. They have devised a classification scheme that helps to understand the features of the drug-like compounds,

dividing them in three classes depending on the calculated barrier and rotation rates, as shown in Scheme 1:

Torsion rotation

Energy barrier (kcal/mol)	$t_{1/2}$	
Atropisomers (no interconversion)	> 30	years	Class 3
Atropisomers (interconversion)	25-30	days-years	Class 2
	20-25	min-hours-days	
Free Rotation	< 20	sec-min-hours	Class 1

Scheme 1. Qualitative, cross-discipline guide to help correlate axial (torsion) rotation energy barriers, $t_{1/2}$, and compound classes for predicting development strategies.

Class 1 compounds possess fast axial rotation rates, in the order of seconds or lower, with $\Delta E_{rot} < 20$ kcal/mol. They display no axial chirality and are developed as single compounds, without any analytical strategy implemented. On the other hand, compounds with $\Delta E_{rot} > 20$ kcal/mol can generate atropisomers.

Class 3 compounds have $\Delta E_{rot} >> 30$ kcal/mol, so they have very slow rotation rates, in the order of years. These compounds are stable over time and can be isolated as optically pure and have an acceptable shelf life. Development can proceed similarly to conventional stereoisomers that results from chiral centers.

Class 2 compounds show axial interconversion with values in the range of minutes, days or months. Their development can be challenging, because stereochemical integrity can be compromised over the time course of drug production, administration to patients and half-lives in vivo. In some cases it may be possible to modify the structure to obtain a more suitable analogue for development, designing related compounds that have slower or faster axial rotation rates. When this is not practical, information on the activity of the separate atropisomers in an appropriate *in vitro* or *in vivo* model may help support the proposed developmental pathway. Information on the rate of equilibration and the equilibrium ratio (for atropisomeric diastereoisomers) is valuable for guiding the scientific and regulatory discussions in preparation for first-in-human studies.

The decision to develop a drug candidate as a purified enantiomer, or a racemate, should be made as early as possible during the optimization stage. If possible, options for dealing with the atropisomeric phenomenon should be developed and implemented at this early drug design stage.

For example, if the barrier to atropisomerization is high (class 3), one should aim to develop the drug as a single, pure and stereochemically stable. This is the case of Telenzepine, a selective muscarinic antagonist, that has found use in the treatement of peptic ulcers.[14]
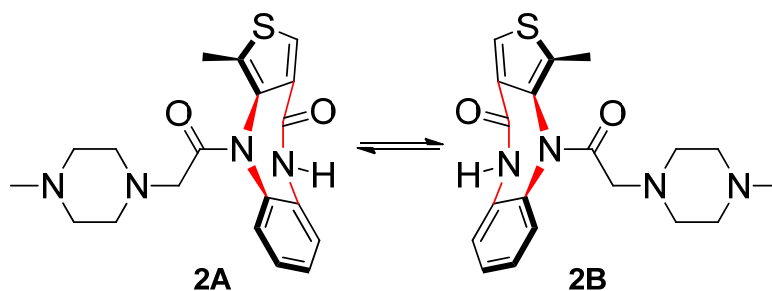
Figure 3. Slow interconversion between the atropisomers of Telenzepine **2A** and **2B**

If the barrier to atropisomerization of a compound is low (class 2), then one should consider developing the drug as a consistent and reproducible interconverting mixture.[15] This is the case for Sch40120 (Figure 4), which is an inhibitor of 5-lipoxygenase. This compound has found use in treating acute inflammatory diseases such as psoriasis.[16]
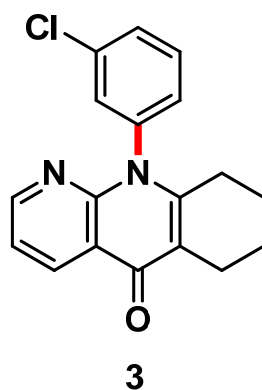
Figure 4. Compound **3** Sch40120 has a fast racemization, of 1.6 min at +37 °C. The rotation axis is colored in red.

In some cases compounds with atropisomeric interconversion properties can be too challenging to be developed as drugs, then for this purpose some practical options can be used to simplify the structure. A related approach to simplification is to modulate the rate of axial bond rotation through engineering faster bond rotation such as atropisomers no longer exist. In this case compounds switch from class 2 to class 1.

Foreseeing the existence of atropisomerism in compounds of interest is critical at all stages of drug discovery and development. Recently, LaPlante and co-workers showed that a computational approach is suitable for this purpose. In this approach, a relaxed torsion scan simulates rotation along a sterically hindered bond and the energy is recorded at each increment of rotation. The method used is quantum mechanics (QM), for the calculation of energy values that consider steric and electronic properties. The computational tool becomes useful during the drug discovery pathway, especially when coupled with the classification scheme mentioned above in Scheme 1, determining whether to develop the drug as a racemic mixture or as an isolated single isomer.

So, it is apparent that atropisomer chirality could have a significant impact on drug discovery and so must be managed appropriately. The first step in dealing with this phenomenon would be to recognize its existence for compounds of interest. The QM torsion profile calculations are a practical strategy for revealing axial energy barriers to rotation that can result in atropisomer properties. Once identified, there are multiple options for dealing with the phenomenon of atropisomerism that can be implemented at the early stage of drug design. For example, it may be possible to make related analogues with the following features: 1) symmetry about a hindered bond, eliminating a chiral axis (making the compound lack atropisomer properties); 2) faster rotation about a hindered bond, pushing the half-life for conformational interconversion down to the order of seconds; 3) further encumbrance about a hindered bond to produce separable atropisomers whose interconversion is negligibly slow (bringing the compound to Class 3); or introduction of a stable stereogenic center to perturb the population of interconverting atropisomers such that only one desirable conformation predominates.[8b]

1.3 Nonbiaryl atropisomers: C-N chiral axis

As mentioned above, over the last two decades there has been a great deal of interest in not only the absolute configuration of stable atropisomeric natural products and drugs, due to hindered bond rotation, but also in their enantioselective, receptor binding properties. This function can be seen as a result of the "adaptability" or "responsiveness" of the stereochemistry of atropisomers. And while the vast majority of atropisomers that have been studied have been carbocyclic biaryls, these form only one of dozens of conceivable families of atropisomers and only during the last 15 years the chemistry of non-biaryl atropisomers has moved beyond simple structural observations.

A number of these non-biaryl atropisomers - diaryl ethers **7**, diaryl ureas, anilides **4**, benzamides **6** and thioamides, styrenes **8** and aryl ketones, *N*-aryl carbamates, aryl sulfides and sulfones, *N*-arylpyrroles **5**, indoles and carbazoles among many more – may offer at least as many benefits in the fields of biology or catalysis as the biaryls themselves.[17]
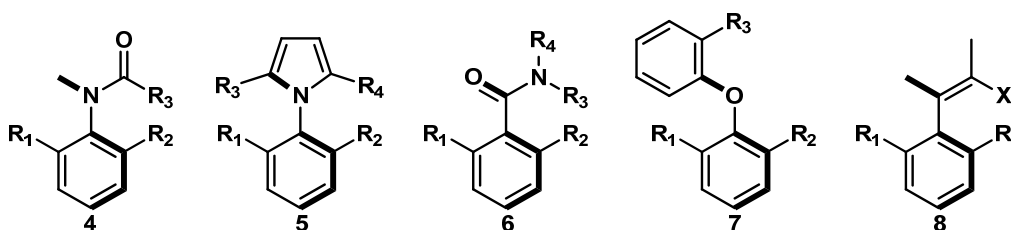
Figure 5 Non-biaryl atropisomers

Few studies regarding the rotation about the chiral sp^2-carbon-nitrogen bond have been reported; in fact there are only few examples of anilides, imides, barbiturates and ureas derivatives.

Mino, Tanaka and co-workers found that the introduction of two different nitrogen substituents to prochiral *ortho*-substituted anilines and 1-aminonaphtalenes provides aryl amines that are axially chiral by virtue of hindered rotation about the aryl-nitrogen bond.[18]

In order to minimize steric repulsion between nitrogen substituents and the aryl ring, N,N-dialkyl arylamines adopt twisted conformations in the ground state.

The interconvesion of the conformational enantiomers of a series of N,N dialkyl-1-naphtylamines[19] and N-aryl tetrahydropirimidines[20] has been studied (figure 6). Notably, concurrent nitrogen inversion of these compounds has a very low energy barrier and is only observable under cryogenic conditions. This greatly facilitates determination of free energy of activation for the rotation about the chiral carbon-nitrogen axis.
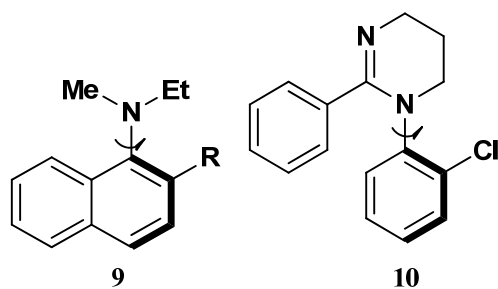
It has been also studied that in order to minimize steric repulsion acetanilides populate a conformation in which the aryl ring and the amide group are orthogonal to each other.[21] As expected the rotation about the axially chiral aryl-nitrogen bond is governed by steric interactions between *ortho* aryl groups and substituents attached to nitrogen atom. In contrast to imides, rhodanines and barbiturates the conformational stability of axially chiral ureas is significantly lower than that of amides, which is attributed to enhanced ground state strain.[22]
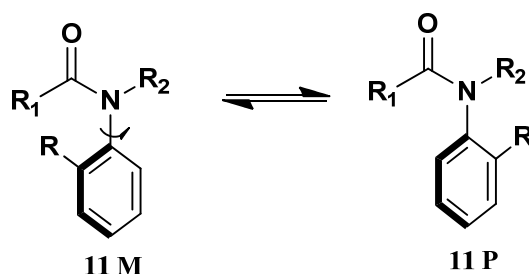
Figure 7 Example of axially chiral anilides

The most studied class of biologically active compounds bearing a C_{aryl}-N chiral axis is that of barbiturates. Oguz and Dogan studied N-O-aryl substituted barbituric and thiobarbituric acid derivatives that are axially chiral due to nonplanar ground states of the molecules.[23] The chiral axis is the C_{aryl}-N_{sp2} bond and all compounds exist as a pair of thermally interconvertable M and P enantiomers. The research group determined the energy barriers of these compounds by either thermal racemization or temperature dependent NMR. They studied ten different structures of barbituric derivatives and they found that oxo-derivatives have a smaller energy barrier compared to that of the thioxo-ones.

Figure 8 The structure of N-*o*-aryl substitued barbituric

The energy barrier for racemization of the *o*-methyl and *o*-chloro derivatives were found to be similar despite of what happens in different types of N-*ortho*-aryl substituted heterocyclic system, such as arylhydantoins, arylquinolones and aryl-rhodanines, where the chlorine atom exerts a greater energy barrier than a methyl group in restricted internal rotation.

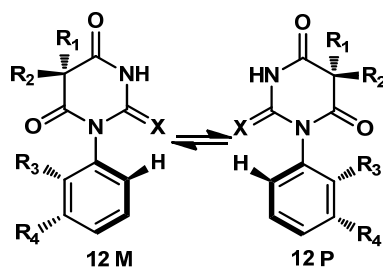These results were explained by dipolar repulsion between the exocyclic oxygen and the chlorine atom. This repulsion might increase the free energy of the transition state of the compound with a chlorine atom as the *ortho* substituent relative to that of the methyl group as the *ortho* substituent. It can be also argued that the difference in the steric effects of these two groups depends on the geometries of the transition states that the two rings assume in passing one another. The tetrahedral nature of the methyl substituent may allow, depending on the geometry, a lower barrier despite its larger reported van der Waals radius[24] than the spherical chlorine atom.

The *o*-fluoro derivative has the lowest energy barrier (ΔG= 22.2 kcal/mol) cause the smallest van der Waals radius of the fluorine atom. On the other hand the naphthyl derivative shows the biggest energy barrier (ΔG= 27.7 kcal/mol).

Pfizer medicinal chemists synthesized one cytokine inhibitor, PH-797804 (**13 P**), that is of particular significance for its excellent kinase selectivity. The PH-797805 (**13 M**) was much less active (figure 9). This atropisomerism arises from restricted rotation caused by the steric bulk of the pyridinone carbonyl and 6,6'-methyl substituents on the pyridinone and N-phenyl rings. The activation energy of the isomeric interconversion between the P and M isomers was predicted to be 31.0 kcal mol^{-1}. Based on the first-order rate equation, the corresponding half-life of the two atropisomers is calculated to be about 111 years at room temperature, making PH-797804 a clinical candidate with excellent in vitro and in vivo activity. Moreover molecular modeling studies indicate that the atropic (*P*)-isomer readily binds within the active site of the kinase. In contrast, the steric clash between the (*M*)-isomer's methyl amide moiety and the protein's Asp112 and Asn115 amino acids prevents access to the active site.[25]
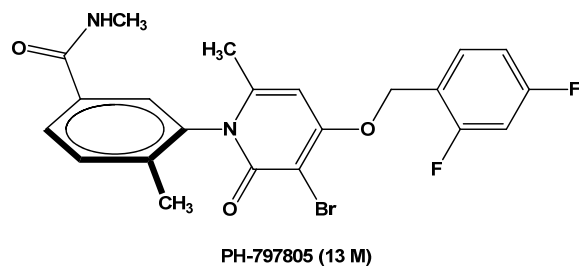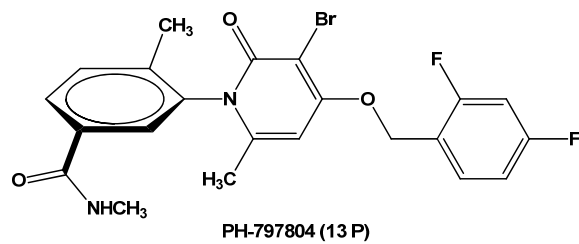
PH-797804 (13 P)

PH-797805 (13 M)

Figure 9 The two atropisomers of cytokine inhibitor

1.4 Xanthines

Xanthine (3,7-dihydro-purine-2,6-dione), is a purine base. Modified purine bases play an important role in biology, and they are interesting systems from biochemical, pharmacological, and chemical points of view. In particular, xanthine exists in both prokaryote and eukaryote cells and participates in a large variety of functions in most human body tissues and fluids.

A number of central nervous system, muscles and cardiac stimulants[26] are derived from xanthine, including caffeine[27] and theobromine.[28]

14	**15**	**16**	**17**
Xanthine	**Caffeine**	**Theophylline**	**Theobromine**
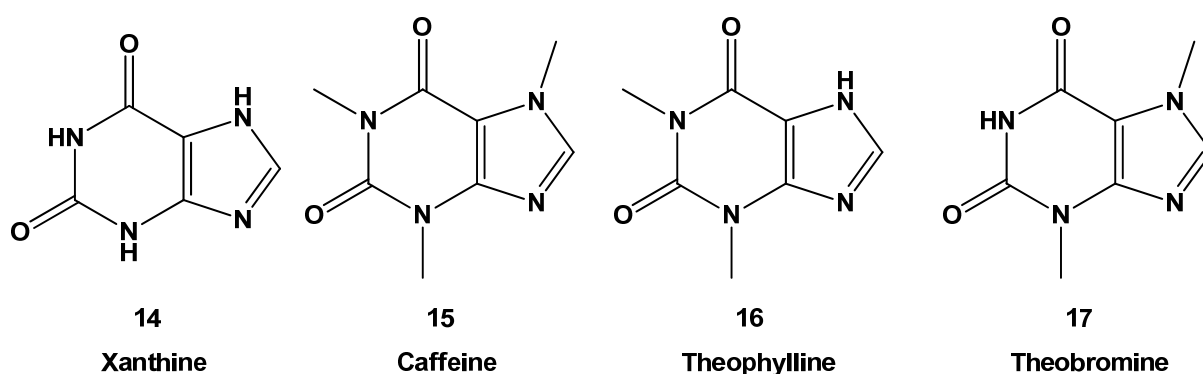
Figure 10 Xanthine derivatives

Xanthine is an intermediate in nucleic acid degradation from the spontaneous or nitrosative deamination of guanine, where the amine group of guanine is substituted by an oxygen atom in xanthine. It is also created from hypoxanthine[29] by Xanthine Oxidoreductase[30] and from xanthosine by Purine Nucleoside Phosphorylase (PNP).[31,32] Xanthine is subsequently converted to uric acid by the action of the Xanthine Oxidase[34] enzyme.

Furthermore, xanthine is a compound present in the ancient solar system. It has recently been demonstrated that this purine is one of the original exogenous nucleobases abundant in prebiotic age on Earth and may have been one of the precursors for nucleic acids.[33]

1.5 Xanthine derivatives

Xanthine derivatives are a group of alkaloids; many of them are naturally occurring drugs that find use as central nervous system stimulants, caffeine being the most famous, one of the most widely consumed, biologically active substances.

1,3-Substituted xanthines constitute an important class of pharmacologically active compounds with well-established activities as not only stimulants, but also phosphodiesterase inhibitors, which increases cellular cyclic AdenosineMonoPhosphate levels, chloride channel activators, and adenosine receptor antagonists. In recent years, the spectrum of clinical applications of these xanthines has continued to widen and presently includes their use as anticonvulsants and therapeutics for the treatment of bronchial asthma and vascular diseases.[34] N3-substituted xanthines, in particular, N3-methylxanthine, an intermediate in the metabolism of methylxanthine alkaloids (caffeine, theophylline, and theobromine), possess interesting properties such as bronchodilator effects, resulting in relaxation of smooth muscle and have been employed to study the dynamics of theophylline-binding RNA aptamers.[35]

The most common used xanthine derivative bronchodilator, in fact, is theophylline, a drug widely used in the management of asthma.

In contrast to other, more potent stimulants like sympathomimetic amine,[36] xanthines mainly act to oppose the actions of the sleepiness-inducing adenosine,[37] and increase alertness in the central nervous system.[38]

All Adenosine Receptor (AR) antagonists are derivatives of the physiological receptor ligand, adenosine. The existence of two types of adenosine receptors has been proposed: an A1 receptor, which mediates inhibition of adenylate cyclase, and an A2 receptor, which stimulates the cyclase. Antagonism of either the AI or A2 receptor would permit the selective control of the effects caused by the binding of adenosine to that particular receptor.[39] The most important class of AR antagonists are the xanthines. Numerous xanthine derivatives, mainly 1,3-disubstituted (theophylline analogs), 1,3,7-trisubstituted (caffeine analogs), and 1,3,8-trisubstituted (8-phenyltheophylline analogs), have been synthesized and investigated in terms of affinity for A1 and A2 receptors and selectivity.

Furthermore, the 1-monosubstituted xanthines were more potent at both receptor subtypes compared to any other monosubstituted xanthines. So, substitution at the 1-position was

necessary for high affinity at adenosine receptors. The 3-monosubstituted xanthines had relatively low affinity for ARs.

The most potent disubstituted xanthines were the l,3-disubstituted analogs of theophylline, particularly at the A1 adenosine receptor. Affinity for AlARs was increased by replacing the methyl groups in theophylline by larger substituents from ethyl to propyl and to isobutyl.[40]
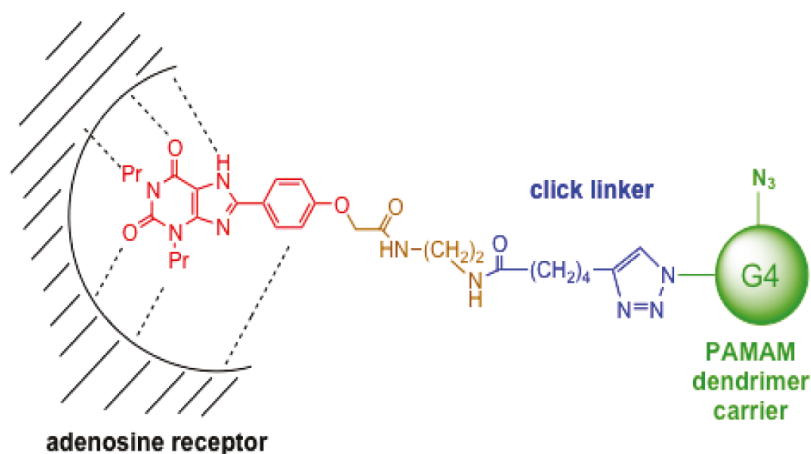
18

Figure 11 Design of a multivalent dendrimer conjugated to a xanthine.

Lyles, Cameron and Rawls found also that caffeine (CAF) may be able to reduce the cytostatic/cytotoxic activity of DNA intercalators agents that share three common properties: (i) they are planar polyaromatic molecules; (ii) they can interact with double-stranded DNA (dsDNA) via intercalation; and (iii) they can form non covalent complexes with planar polarizing compounds such as CAF. When added simultaneously with or immediately before the intercalating agent, CAF has been reported to diminish the cytotoxic effects of the hemotherapeutic drugs doxorubicin (DOX) and novantrone in a variety of cell lines. Additionally, CAF reduced the cytotoxicity of the DNA intercalator, ethidium bromide, by reducing its ability to enter cells. The proposed mechanism responsible for the reduction in cytotoxicity by DNA intercalators is the formation of a noncovalent complex between the xanthine and the intercalator.[41]

In conclusion xanthine and its derivatives had always interested the field of chemistry and biochemistry as molecules of study for creating potentially different kind of drugs, thanks to their singular biological activities. As a result, the attractive studies on these molecules are still in progress; in fact we choose to focus our attention on different atropisomeric xanthines derivatives to study in detail this kind of bioactive compounds.

2. Results and discussion

During these last decades there has been an increasing interest towards pharmacologically bioactive compounds showing atropisomeric features. In particular, the main research goal is to synthesize bioactive compounds with conformational chirality due to a rotational energy barrier higher than 30 kcal/mol, where the conformers are stable at room temperature with a half-life time in the order of years.[42] This is a very important feature to reach because the pharmacological properties of axially chiral bioactive compounds are directly related to their stereodynamic processes.

The aim of my experimental thesis is the preparation of stable atropisomers of xanthines and the resolution of the enantiomeric forms, which could be used in the field of drug discovery.

To investigate the feasibility of atropisomeric xanthines, three different compounds were synthesized following the synthetic scheme reported below: (see *Experimental* procedure for further information)
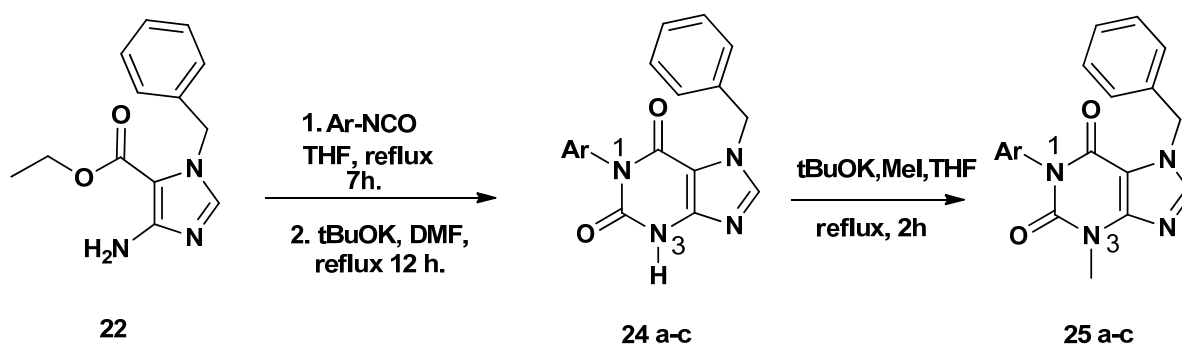
Figure 22 Synthetic scheme for xanthine derivatives: 24a) Ar = *o*-tolyl; 24b) Ar = *o*-nitro phenyl; 24c) Ar = naphthyl

Xanthines **25a-c** were prepared following literature procedures[43] that involve the nucleophilic attack of the primary amine to aryl isocyanate giving as intermediate a N-aryl-substituted urea that is consequently deprotonated by means of a strong base to achieve the six-membered ring closure, leading to the desired purine structure. The final step is the N-3 methylation using methyl iodide as methylating agent (figure 22).
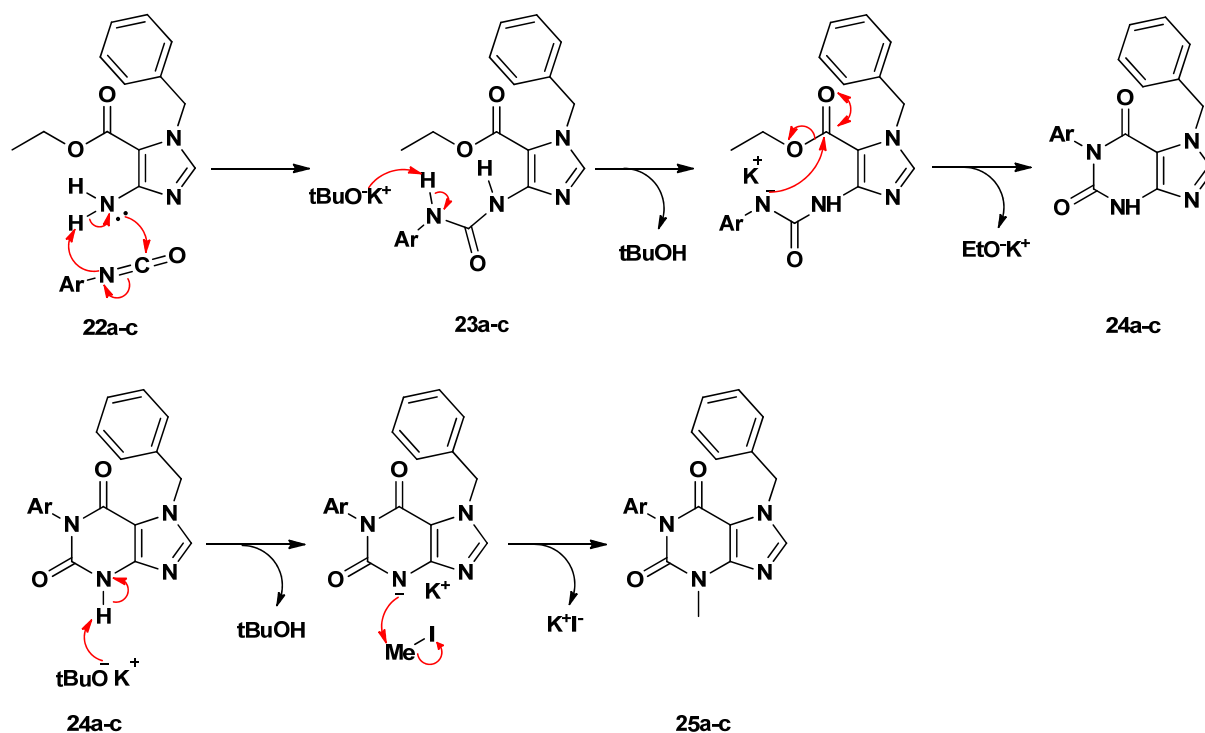
Scheme 2 Synthetic mechanism to achieve compound 25a-c

Xanthine scaffold is a planar framework and the *ortho*-substituted aryl in the 1-position is driven out of the xanthine plane because of the steric hindrance caused by the ortho substituent. This arrangement implies tilted conformations that generate conformational chirality. Depending on the hindrance of the *ortho*-substituents, the resulting conformational enantiomers can be either stereo labile or configurationally stable (atropisomers). Preliminary theoretical studies by DFT calculations support indeed the existence of a pair of M and P conformational enantiomers, due to the skewed dispositions adopted by the $R_{1,2}$ substituents of aryl-group that can stay up or down the xanthine planar scaffold.

In figure 13 the two available ground states are reported.

Figure 13 The two possible enantiomeric conformations
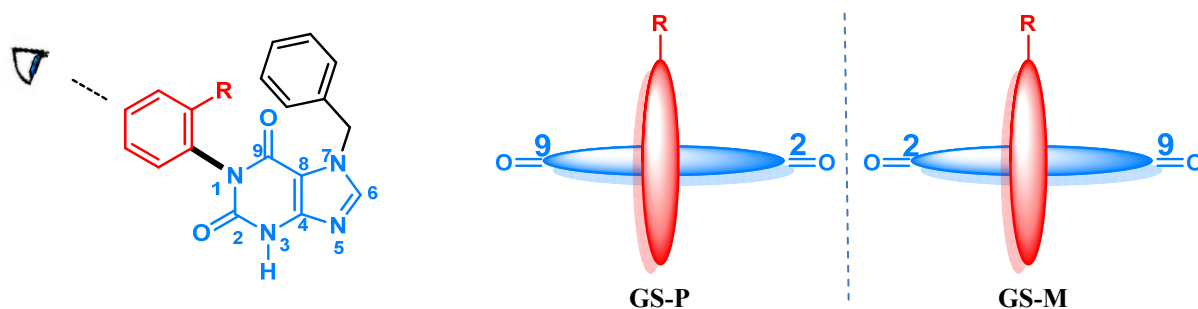
The interconversion pathway between the two conformational enantiomers can take place through two different transition states, depending on the side of the rotation of the R group around the C_{sp2}–N chiral axis, through the two different carbonyl moieties (figure 14):
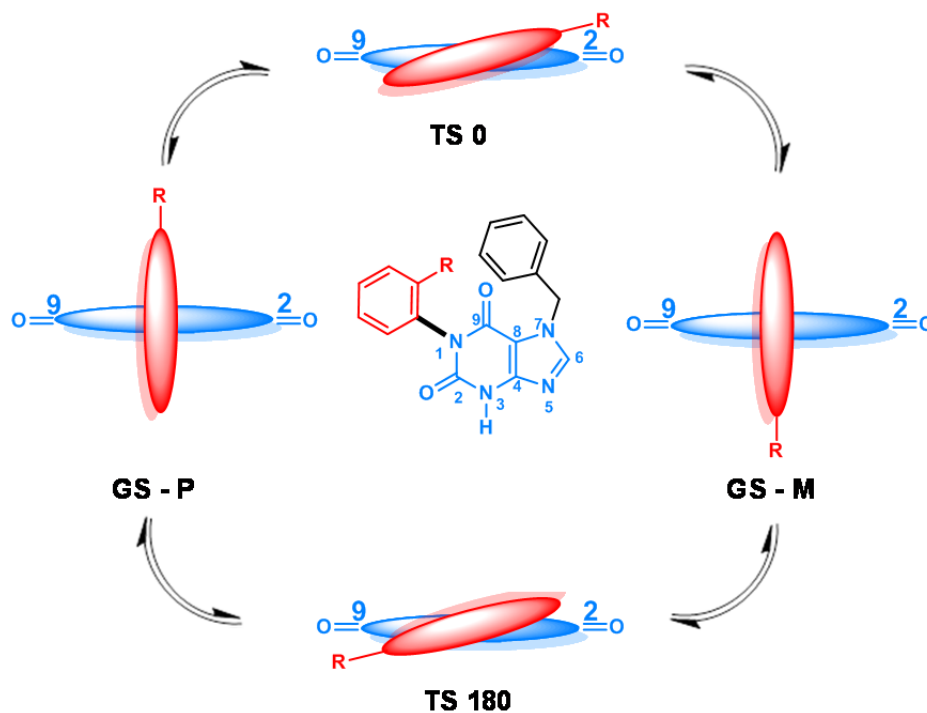
Figure 14 Schematic rotation of aryl group about the chiral axis

TS0 represents the transition of the aryl *ortho* substituent on the side of the carbonyl group in position 2 of xanthine scaffold, while the TS180 the crossing of the same substituent on the side of the other carbonyl group in 9 position. Depending on the hindrance of the *ortho* substituent on the aryl group, the transition states may be characterized by different values of interconversion energy barrier ($\Delta G^{\neq}$). A well known approach to analyse the presence of a pair of unstable and stable atropisomers is dynamic-NMR spectroscopy. In the present case the two conformations are enantiomeric, and their occurrence could be revealed by using a CSA (Chiral Solvating Agent), or by the presence of a chirality probe containing two germinal moieties that shows diastereotopic signals when conformational enantiomers are formed. To avoids the drawback that hampers the use of CSA, we decided to add a chirality probe to the xanthine scaffold. To avoid any steric interference with the 1-aryl group, a benzyl group was bonded to the nitrogen in position 7 of the xanthine scaffold. This group was chosen for the presence of an uncoupled CH_2 group that acts as the chirality probe, thus

displaying diasterotopic signals (AB system) only when the motion is frozen in NMR timescale and a pair of conformational enantiomers has been developed.

In figure 15 is shown a representation of the effect of the molecular motions on the CH_2 NMR signal. When the rotation of the aryl group is fast, only a single averaged signal is visible (^{1}H-NMR spectrum on the top in figure 15). When the rotation of the aryl is slow in the NMR timescale (bottom ^{1}H-NMR spectrum in figure 15), the benzyl CH_2 act as a chirality sensor displaying a double doublet (AB system), due to the different magnetic environment of the two diastereotopic hydrogens.
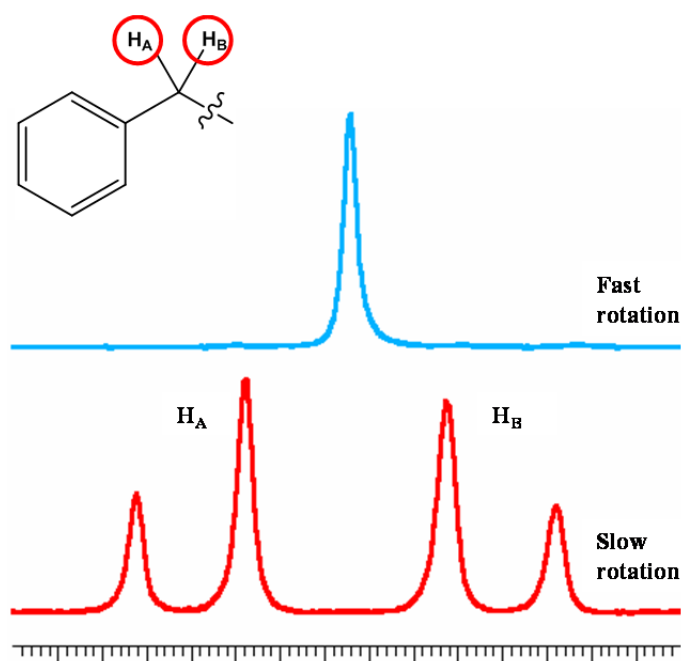
Figure 15 Representation of AB spin system relative to benzyl CH_2 at fast and slow rotation.

2.1 Stereodynamic: rotational energy barrier

In the figure below the six synthesized xanthine structures are shown. The 1-aryl-substituents are represented by increasingly *ortho* bulky groups, to achieve the freezing of rotation motions.
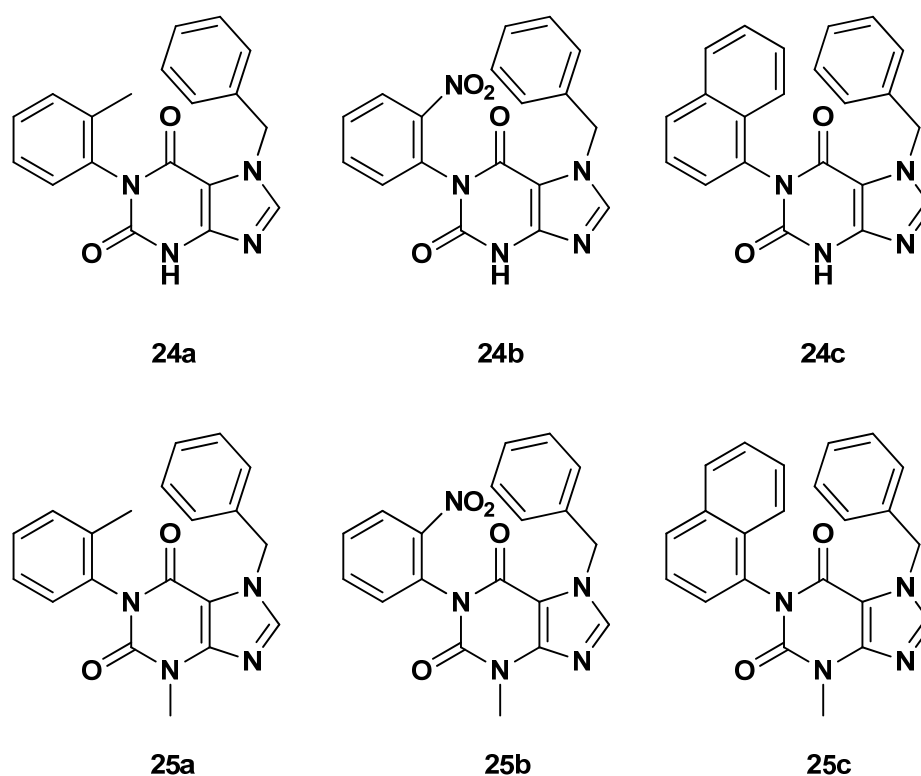
Figure 16 Atropisomeric xanthine derivatives

The stereodynamic pathways of each conformer was theoretically modelled by DFT optimization performed using Gaussian 09 and the B3LYP/6-31G(d) level of theory, that proved to be quite accurate in similar cases. Both ground and transition states were obtained (see *Appendix* for more theoretical details) by full optimization and validated by frequency calculation.

DFT calculations can perform a reliable conformational analysis, useful to predict and confirm the relative energies of the ground and transition states, allowing us to choose the best experimental approach to study the stereodynamic processes. In addition to that, the determination of relative energies among the available transition states gives conformational information about the most favourable stereodynamic pathway. The lower value of transition state energy, in fact, represents the effective mechanism of interconversion between two fundamental states. It is important to stress that only the ground states, and not the transition

states, can be experimentally observed, so the effective transition state is deduced only *via* the theoretical simulation.

Depending on the relative disposition of the benzyl group with respect to the *ortho*-substituent of the 1-aryl ring, two different conformations rise up: they are named *syn* and *anti*. The *syn* conformation puts the phenyl ring of the benzyl group on the same side of the *ortho* substituent with respect to the xanthine core, whereas the anti conformation puts the phenyl of the benzyl group on the opposite side. A total of four conformations (two pairs of diastereoisomer) have therefore to be considered.

In addition to that, DFT calculations suggested that the N-1-aryl ring is not exactly perpendicular to the xanthine scaffold, so two additional conformations have to be considered for each *syn* and *anti* conformer. The four conformations relative to the M atropisomer are shown in figure 17.
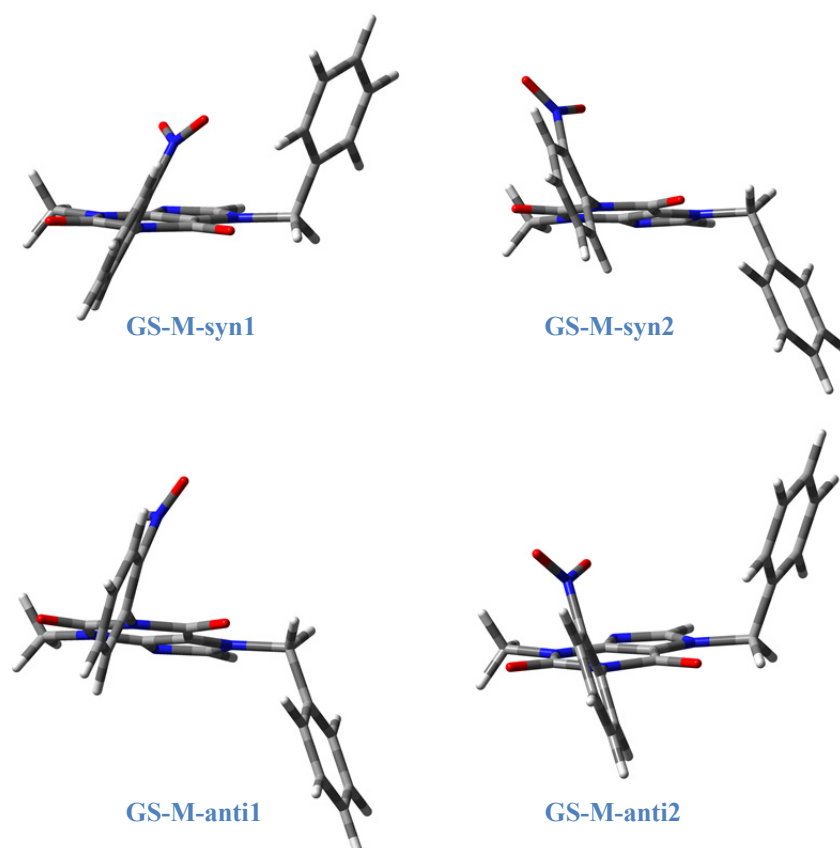
Figure 17 Compound 25b: GS-M-syn1, GS-M-syn2 (top), GS-M-anti1, GS-M-anti2 (bottom)

In table 1 are reported the energy values for both ground and transition state, regarding the *M* enantiomer, derived from DFT calculations. The ground states taken into account are clustered into a very small energy range, the highest energy being about 1 kcal/mol above the

global minimum. The small energy range implies that all the conformations should be appreciably populated.

Table 1 Optimized ground and transition states normalized energies of the atropisomer M, expressed in kcal/mol, calculated at B3LYP/6-31G(d) level; the enantiomer P has the same energy values.

Entry	GS-M-syn1 D[a] (%)[b]	GS-M-syn2 D[a] (%)[b]	GS-M-anti1 D[a] (%)[b]	GS-M-anti2 D[a] (%)[b]	TS0-Bn up	TS180-Bn up	TS0-Bn down	TS180-Bn down
24a	0.00 -79.08° (49.8)	-	0.00 -84.47° (50.2)	-	27.58	27.90	27.45	27.94
24b	0.00 -113.08° (34.6)	0.30 -69.77° (20.9)	0.212 -105.81° (24.2)	0.317 -70.25° (20.3)	25.24	24.59	25.15	23.53
24c	0.00 -92.80$_5$° (53.5)	-	0.08 -91.19° (46,5)	-	30.171	30.471	30.117	30.693
25a	0.00 -79.42° (29.4)	0.169 -80.46° (22.1)	0.02 -82.26° (28.2)	0.22 -97.08° (20.3)	28.08	28.19	27.87	28.27
25b	0.00 -112.59° (32.3)	0.22 -68.82° (22.3)	0.19 -104.43° (23.5)	0.23 -68.75° (21.9)	25.27	23.76	25.12	24.78
25c	0.00 -89.59° (52.7)	-	0.06 -91.16° (47.3)	-	30.66	30.74	30.53	31.04

[a] *Dihedral angle values*

[b] *Percentage of each populated state*

Compounds **24c** and **25c**, bearing a naphthyl group, shows only two different ground states, because the higher hindrance drives the dihedral angle to 90° (figure 18).
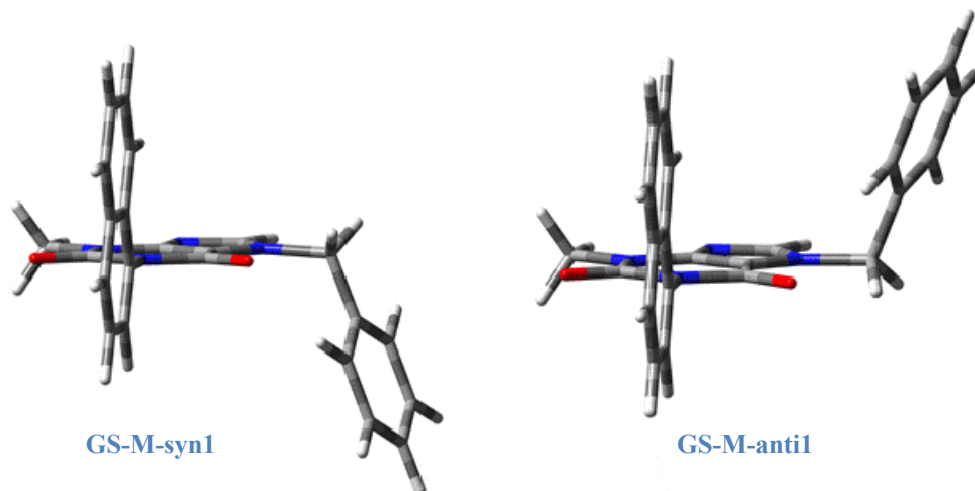
GS-M-syn1   **GS-M-anti1**

Figure 18 Compound **25c**: GS-M-syn1, GS-M-anti1

Conformation GS-syn-1 represents for compounds **25a, 25b, 25c** the lowest energy state, indicating that the most energetic favourable states is that where the substituted aryl ring is on the same side of the phenyl of the benzyl moiety. The most energetically favourable ground state of compound **25a** is that characterized by the smallest dihedral angle (compound **25a**: $\varphi_{GS-M-syn1}$= -79.42°); while GS-M-syn1 of compound **25b** shows a dihedral angle $\varphi_{GS-M-syn1}$= -112.59°, that is bigger than 90°.

Depending on the relative disposition of the benzyl moiety (i.e. up or down the planar xanthine scaffold) and on the side where the substituted aryl passes during the rotation around the chiral axis, four transition states are possible, as shown in figure 19.

TS0-Bn up
$\Delta G^{\neq}$ = 28.08 kcal/mol

TS180-Bn up
$\Delta G^{\neq}$ = 28.19 kcal/mol

TS0-Bn down
$\Delta G^{\neq}$ = 27.87 kcal/mol

TS180-Bn down
$\Delta G^{\neq}$ = 28.27 kcal/mol
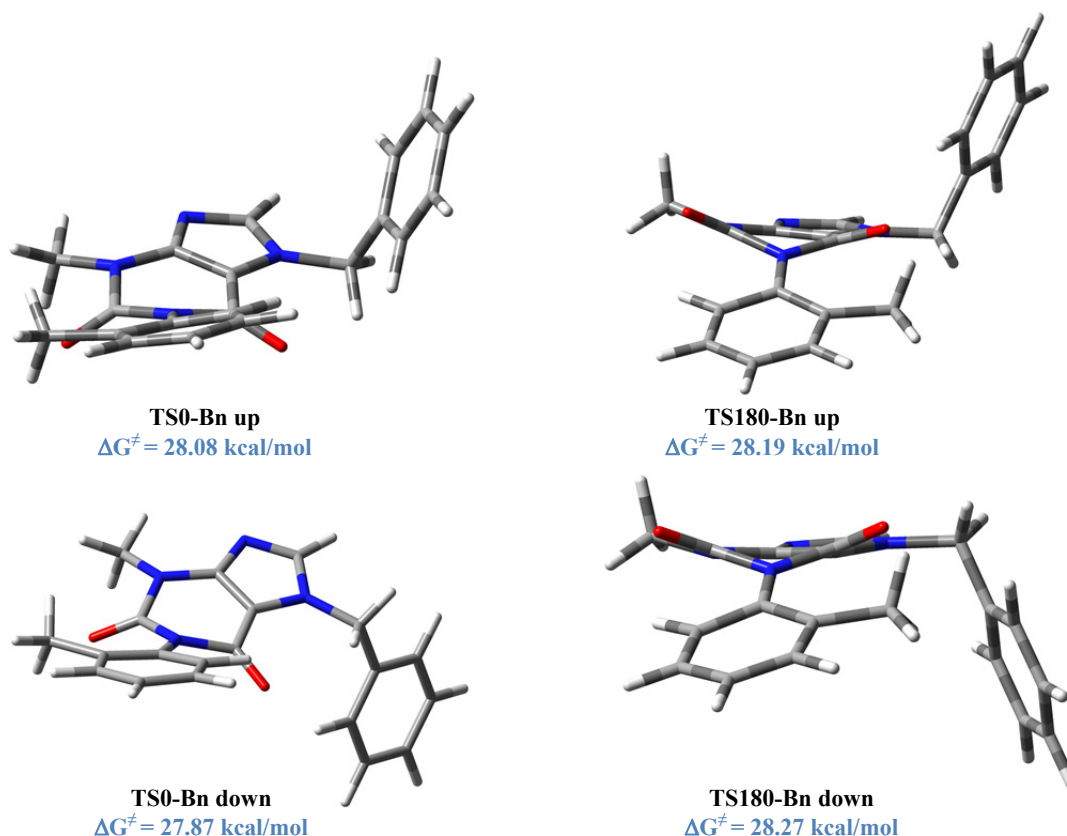
Figure 19 Transition states of compound 25a, TS0-Bn down is the most stable

As from table 1, compound **24a**, **24c**, **25a** and **25c** prefer the passage on the side of the carbonyl in position 2 and with the benzyl group down the xanthine plane, but the energies are very close and a reliable conclusion cannot be extracted. On the other hand, the suggested energies are rather high, and they should allow for the formation of stable atropisomers. The transition states of compounds **24a, 24b, 24c** with respect to **25a, 25b, 25c** are very close in energy, suggesting that there is no influence in the energy barrier when the xanthine core bears a *N*-Methyl group instead of a N-H. While compound **25b**, characterized by the *o*-nitro phenyl substituent, shows as energetically favourable the transition state TS180-Bn-up, that involves the crossing on the side of the carbonyl in position 9 and the benzyl group up the planar scaffold (figure 20).

TS 180- Bn up
$\Delta G^{\neq}$=23.76 kcal/mol
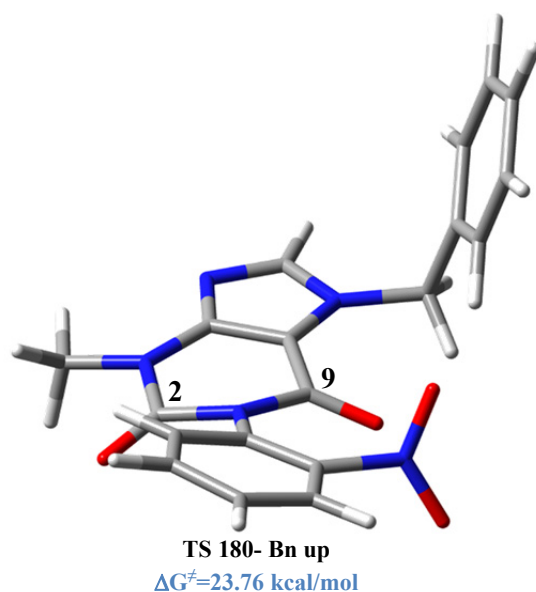
Figure 20 Most stable transition states of compound **25b**

We found surprisingly a calculated energy barrier lower than the one relative to the compound **25a** for compound **25b,** that has a nitro group isosteric with the methyl moiety,[44] (23.76 kcal/mol). The rotation rate of interconversion may be influenced not only by steric hindrance, but in this case by electronic factors too. As shown in figure 20 representing the TS180-Bn-up, an electronic interaction rises up between the electron-rich oxygen of the carbonyl moiety and the electron poor nitrogen of the nitro group. This interaction can stabilize the transition state thus lowering the rotational barrier. These theoretical results must be supported by the experimental approach, though.

As from the calculations, all the compounds should feature a $\Delta G^{\neq}$ value higher than 25 kcal/mol, so they should be conformationally stable at ambient temperature. A first test on compound **24a** was done by using an enantioselective HPLC column (ChiralPak AD-H). The chromatogram showed the elution of broadened and closed peaks relative to the two enantiomeric conformers. The presence of a secondary free amine group lead often to broadened chromatographic peaks, because of its interaction with the stationary phase. Although this confirmed the presence of atropisomeric compounds, the peak broadening did not allow us a good separation and consequently a good kinetic studies to determine the energy barrier.

To solve this problem we decided to protect the free amine with a methyl group that doesn't interfere with the rotation around the chiral axis, but that allowed us to purify each atropisomer without committing any mistakes due to a difficult elution step.

Compounds **25a** and **25c** were purified, using an enantioselective HPLC, by means of ChiralPak AD-H column, while the atropisomeric **25b** was purified with Lux Cellulose 2 column (see *Experimental section* for further details) using different ratio of Hex : *i*PrOH as elution mixtures (table 2).

Table 2 Elution conditions: compounds 25a and 25c were purified using an enantioselective HPLC by means of AD-H column, while 25b was eluted using Cellulose2 column

Entry	Elution mixture (Hex : *i*PrOH) (v/v)
25a	80:20
25b	50:50
25c	76:24

Once purified each atropisomer, all the compounds were subjected to kinetic studies at different temperatures to obtain the experimental value of the energy barrier of interconversion.

The racemization process, i.e. the thermal equilibration of the two atropisomers was followed by means of chiral HPLC (i.e. ChiralPak AD-H column and Lux Cellulose 2 column), with the same elution conditions used in the purification step (table 2).

The kinetic analysis of all the atropisomeric molecules were performed using the same experimental approach. An aliquot of a pure enantiomer was dissolved in 1 mL of $C_2D_2Cl_4$ using a test tube with screw cap. After that the phial was kept into a bath of DMSO surrounded by an oil bath, placed on a hotplate magnetic stirring. The oil bath is necessary to keep the temperature controlled by means of a thermocouple put in DMSO solution. The choice of $C_2D_2Cl_4$ was made because its high boiling point that is +146.5 °C, still with a good vapor pressure that allows to easily evaporate it. Small samples were taken at different times, evaporated the solvent and analyzed by enantioselective HPLC that allowed the determination of the enantiomeric ratio.

Once complete racemization was reached, the experimental values were collected and interpolated by a first order reversible kinetic equation and the rate constant (*k*) values referred to each experimental temperature were obtained.

$$M \underset{}{\overset{k}{\rightleftharpoons}} P$$

$$\ln (x - x_{eq}) = \ln (x_0 - x_{eq}) - 2 k t$$

Where x is the molar fraction of the enantiomer that is interconverting; x_{eq} is the molar fraction of the same enantiomer reached at the equilibrium state (0.5); x_0 is the initial molar fraction of the chosen enantiomer at t_0; k is the rate constant (s^{-1}); t is the time steps (s). This equation represent a straight line in the form $y = mx + q$, where the slope is *(-2k)*; the y-intercept is *ln (x_0-x_{eq})* and t is the independent variable of the function.(see *Appendix* for complete demonstration)

The resulting k values, not dependent upon concentration, were then used to derive the free energy of activation ($\Delta G^{\neq}$ in kcal/mol) at each temperature by means of the Eyring equation,[45] where T is the absolute temperature and k is the rate constant in s^{-1}:

$$k = k \frac{k_B \cdot T}{h} e^{-\frac{\Delta G^{\neq}}{RT}}$$

h = Planck's constant ($1.584 \cdot 10^{-34}$ cal·s)

k_B = Boltzmann constant ($3.2998 \cdot 10^{-24}$ cal/K)

R = universal gas constant (1.9872 cal/K·mol)

κ = transmission coefficient (can be considered equal to 1)

Solving for $\Delta G^{\neq}$ in kcal/mol:

$$\Delta G^{\neq} = 4.574 \cdot 10^{-3} \cdot T \cdot (\log \frac{T}{k} + 10.318)$$

Table 3 shows the racemization trend at the temperatures chosen for the kinetic studies of the compound **25a** (Figure 22).(see *Experimental section* for the other compounds).

| t=0 s | t=1800 s | t=3600 s | t=6660 s | t=10980 s |
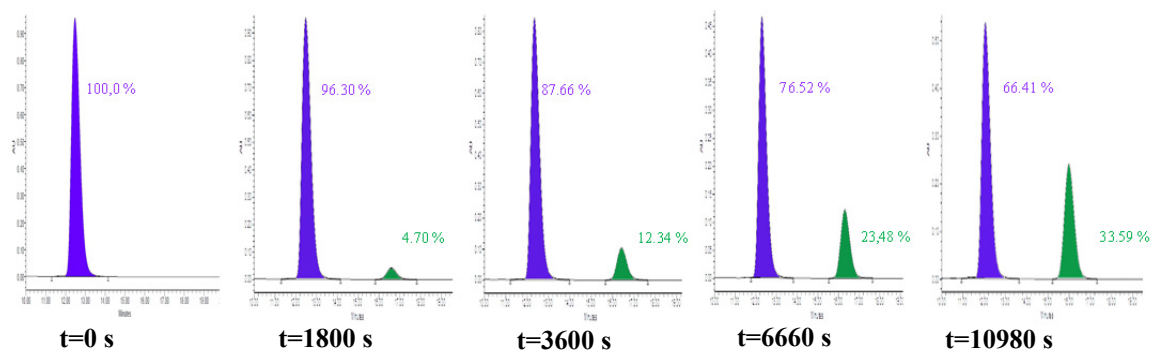
Figure 21 Example of racemization followed by enantioselective HPLC AD-H of compound 25a at +115°C

Table 3 Compound 25a: Racemization process at each temperature of first eluted atropisomer

T +100 °C		T +105 °C		T +110°C		T +115°C	
t (s)	$\ln(x_{ena1}-x_{ena1\_eq})$	t (s)	$\ln(x_{ena1}-x_{ena1\_eq})$	t (s)	$\ln(x_{ena1}-x_{ena1\_eq})$	t (s)	$\ln(x_{ena1}-x_{ena1\_eq})$
0	-0,69315	0	-0,69315	0	-0,69315	0	-0,69315
2520	-0,75184	3420	-0,81058	4620	-0,98967	1800	-0,79186
4380	-0,82098	6840	-0,92659	8160	-1,212	3600	-0,97657
9240	-0,96601	10140	-1,05872	11580	-1,42753	6660	-1,32727
12720	-1,03818	13440	-1,19106	15480	-1,68201	10980	-1,80728
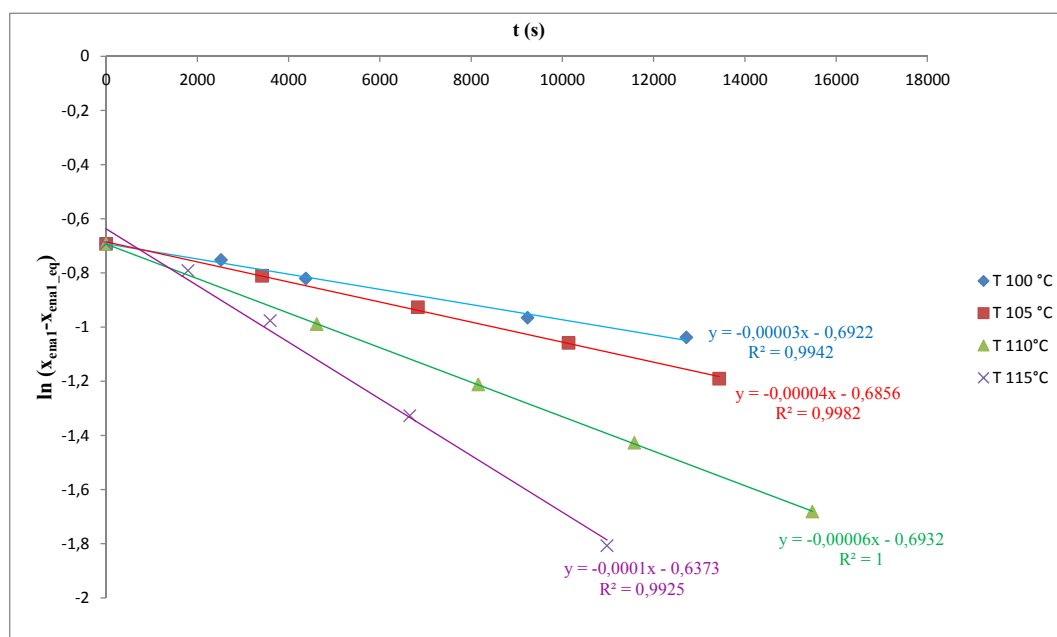
Figure 22 Compound 25a: Kinetic data fitted with linear regression relative to thermal racemization of first eluted atropisomer

As we can notice from the graphic and table, the experimental values follow a good linear trend typical of the kinetic of first order, so they can be reliably interpolated with a linear regression to calculate the constant rate values (k).

Once obtained the k values, the $\Delta G^{\neq}$ were calculated through the Eyring equation and the results are collected in table 4.

Table 4 Compound 25a, 25b, 25c: Rate constants and activation energies of interconversion

COMPOUND 25a	T +100 °C	T +105 °C	T +110 °C	T +115 °C
k (s^{-1}) (x10^{-5})	1,40	1,87	2,95	5,23
$\Delta G^{\neq}$ (kcal/mol)	30,29	30,49	30,56	30,53
COMPOUND 25b	**T +30 °C**	**T +50 °C**	**T +56 °C**	**T +58 °C**
k (s^{-1}) (x10^{-5})	0,47	4,50	9,67	9,19
$\Delta G^{\neq}$ (kcal/mol)	25,15	25,39	25,38	25,57
COMPOUND 25c	**T +100 °C**	**T +110 °C**	**T +120 °C**	**T +130 °C**
k (s^{-1}) (x10^{-6})	0,79	2,47	6,85	17,74
$\Delta G^{\neq}$ (kcal/mol)	32,42	32,45	32,52	32,60

Taking into account the errors in the determination of the sample temperature (±1°C), the free energies can be considered invariant with the temperature, thus implying a negligible activation entropy. This is usual in conformational processes.[46] Therefore, the average $\Delta G^{\neq}$ is carried out to eliminate all the possible experimental errors and these values were compared with the calculated. (table 5)

Entry	$\Delta G^{\neq}_{exp}$ (kcal/mol)	$\Delta G^{\neq}_{calc}$ (kcal/mol)	$t_{\frac{1}{2}}$ (+25 °C)	$t_{\frac{1}{2}}$ (+37 °C)[a]
25a	30.5	28.08	77 years	74 years
25b	25,4	23.76	5 days	5 days
25c	32,5	30.53	2353 years	2262 years

[a] Normal human body temperature

We can also observe that the experimental energy value is always in agreement with the calculated one, with a difference less than 2 kcal/mol, typical for this kind of DFT calculation.

So it can lead us to conclude that, as supposed before analyzing DFT optimized conformers, the increasingly bulky substituents of the aryl group (methyl and naphthyl moieties) increases the rotation about the chiral axis, giving as a result a larger $\Delta G^{\neq}$ of interconversion, essential for bioactive atropisomeric compounds. Moreover the experimental values of *o*-nitro phenyl substituent does confirm a lower activation energy with respect to the isosteric *o*-methyl phenyl moiety. As speculated above regarding the calculated energy barriers, the activation energy of the *o*-nitro derivative is lowered by the presence of electronic interactions in transition state between this group and the two carbonyls of the xanthine planar scaffold.

From a pharmacological point of view it is very important to take into account the half-life time of each atropisomeric compound, that is an essential parameter to consider when a bioactive atropisomeric molecule is developed in the field of drug discovery. Therefore we have reported the half-life time at room temperature and at +37 °C that is the normal human body temperature.

Applying the reversible first order kinetic equation the half-life time of each compound is:

$$t_{\frac{1}{2}} = (\ln 2) / k$$

Looking at the energy rotational barrier and half-life time values at room temperature we can affirm that compound **25a** and **25b** belong to the Class 2 of LaPlante classification scheme (scheme 1), while **25c** is more stable and so is relative to LaPlante's Class 3 (see *Introduction* for further details).

2.2 Absolute configuration

Once the stereodynamic behavior and thus the conformational stability of each atropisomeric structure has been analyzed, the absolute configuration was assigned. The "reference" method to assign the absolute configuration relies on the X-ray anomalous scattering (the "Bijvoet method"). However, this approach requires the preparation of enantiopure single crystals, and the presence of an heavy atom in the molecule (usually Z>Si when Mo-Kα radiation is used). In this case the molecules do not contain any heavy atom, and the assignment by X-ray crystallography is unfeasible.

In the last years the determination of the absolute configuration of chiral molecules using chirooptical techniques like optical rotation (OR), electronic circular dichroism (ECD), and vibrational circular dichroism (VCD) gained feasibility and reliability because of the development of theoretical methods for the prediction of these properties based on DFT and on the time-dependent density functional theory approach (TD-DFT).[46,47]

In the present case the theoretical calculation of ECD spectra was selected for the absolute configuration assignment of all the compounds. The conformational search performed on all the atropisomeric structures, showed that **25c** has two populated conformations (*syn* and *anti*), depending on the position of the benzyl compared to that of the naphthyl with respect to the xanthine core, whereas compounds **25a** and **25b** have four ground states conformations for each atropisomer (see table 1).

To compare the calculated ECD spectra to the experimental one, all the populated conformations must be considered and their spectra weighted by means of the Boltzmann equation, so that the final spectrum takes into account all the contributions.

The theoretical ECD spectrum of all optimized ground state conformations was obtained with the TD-DFT method at CAM-B3LYP[48]/6-311+G(2d,p) level (see *Appendix* for further details) because this level of theory has been successfully applied to similar cases.[49]

The experimental ECD spectra were recorded at +25 °C in acetonitrile solution, using a JASCO J-810 spectropolarimeter. The figure below shows both the experimental UV/Vis and the ECD spectra of compound **25c**.

UV/Vis spectrum
compound 25c

ECD Experimental spectrum
second eluted enantiomer
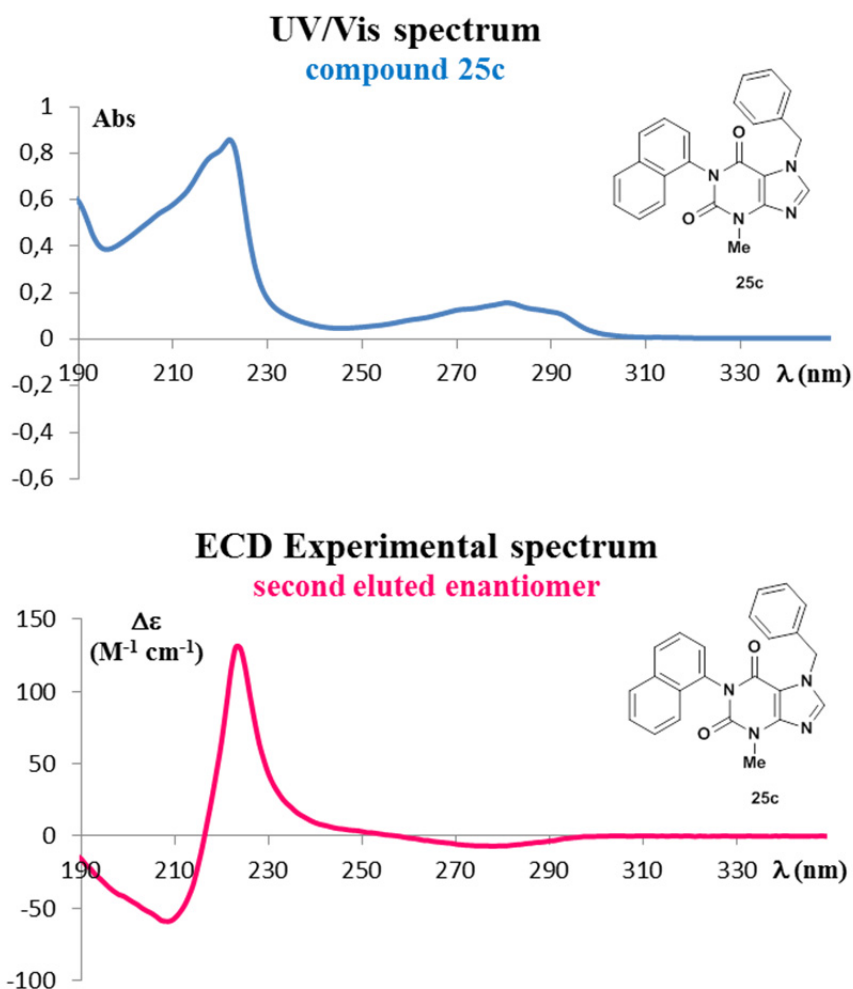
Figure 23 Experimental UV/Vis and ECD spectra of compound 25c

The ECD spectra calculated for **25c** are showed in figure 24, we can notice that the curve is characterized by three Cotton effects: one positive that leads to a maximum related to the absorption band at 221 nm and two negative which cause the formation of two minima respectively at 270 nm and 203 nm.

The bisignate CD arises because the transition moments of chromophores of the atropisomeric compound generate an exciton-coupling. The signs of this curve reflect the chirality between the electric transition moments of the interacting chromophores and are ascribable to a different absorption of the left and right handed polarized light.
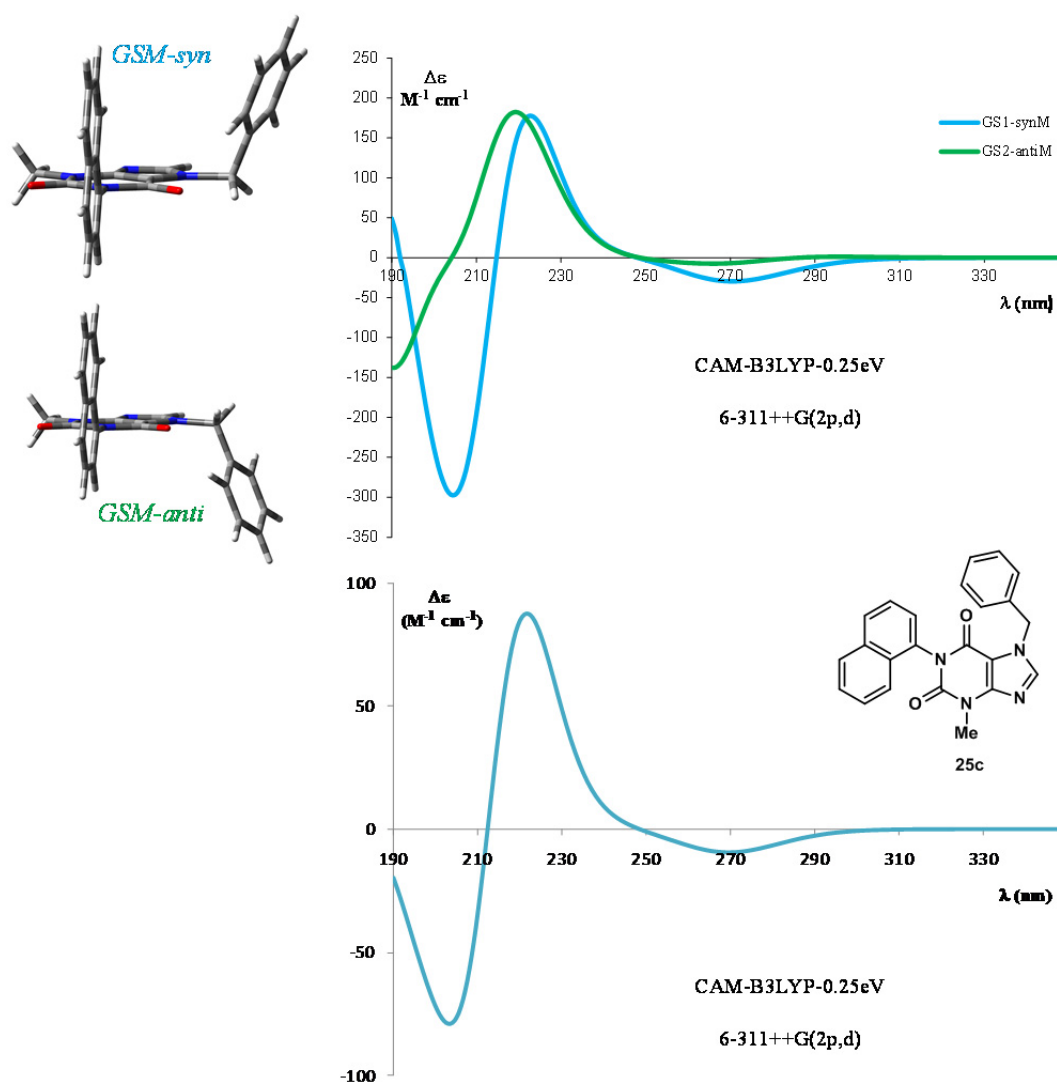
Figure 24 Compound 25c: up GS-M-*syn* and GS-M-*anti* conformations at the left; ECD calculated spectra of GS-M-syn and GS-M-anti at the right. Down ECD calculated spectrum, it is the result of the weighted sum of GS-M-*syn* and GS-M-*anti*

An investigation of the molecular orbitals (MO) involved in the UV transitions that generate these ECD bands confirmed that the small band centered at 270 nm is mainly generated by MOs that involve both the carbonyls of the xanthine scaffold and smaller contributions come from MOs involving the naphthyl ring and the benzyl group. The band at higher excitation energies centered at 221 nm is due to the electronic transitions that implicate mainly the MOs of the naphthyl moiety, but also of the purine scaffold, in particular considering the MOs of the five-membered aromatic ring and the CO in position 2 and 9; there is also a smaller contribute deriving from the MOs of the phenyl ring. The same happens in the high energy band at 203 nm mainly imputable to MOs regarding naphthalene and six-membered ring of

xanthine. Also in this case there is a smaller contribution that comes from MOs of the entire xanthine moiety and the phenyl ring.

Table 6 Calculated MOs of compound 25c

GSM-syn	Exc. State	Wavelength	Oscillator strength	Rotation rate (10^{-40} esu^2 cm^2)	MO	%
	16	199.52 nm	0.4127	-441.98	98→108	17.65
					99→106	12.55
					98→107	11.95
	11	208.74 nm	0.9284	396.38	98→101	39.28
					100→108	23.06
					100→107	16.84
	3	259.38 nm	0.1508	-69.05	99→102	80.18
GSM-anti	Exc. State	Wavelength	Oscillator strength	Rotation rate (10^{-40} esu^2 cm^2)	MO	%
	27	191.60 nm	0.0797	62.216	99→107	29.29
					99→103	6.38
	16	199.64 nm	0.3158	-57.085	98→108	24,50
					99→105	15,54
					97→102	5,46
	15	202.74 nm	0.0830	148.935	100→117	37,31
					100→118	27,69
	11	208.83 nm	1.0852	137.246	100→108	45,20
					98→101	43,62
	3	259.4 nm	0.1450	-21.854	99→102	81,89
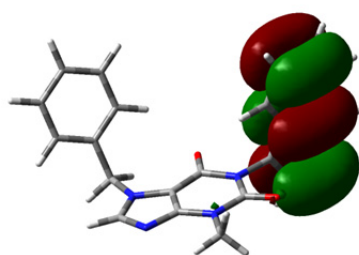
98
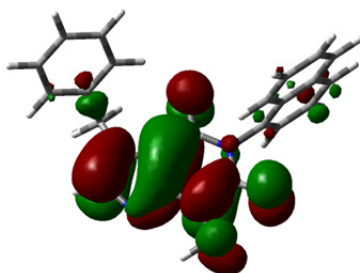
99
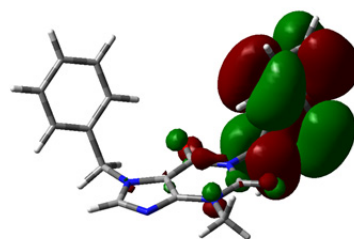
100
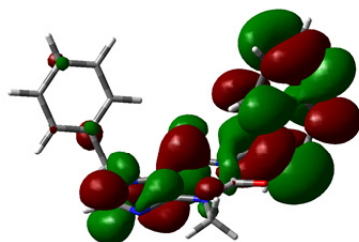
101

102

106

107

108

GS-M-anti

97

98

99

100

101

102

103

105

107

108

117

118
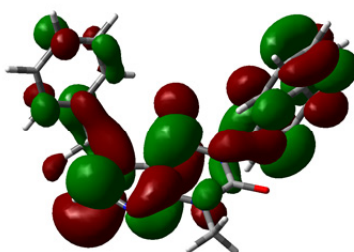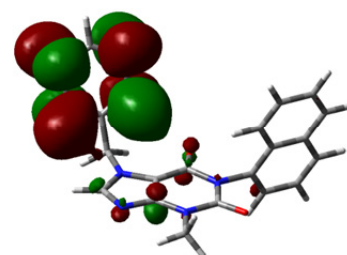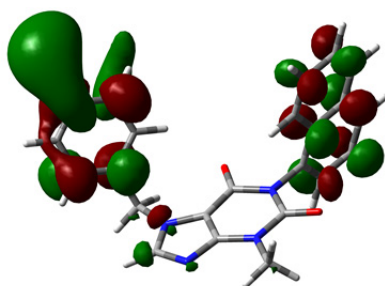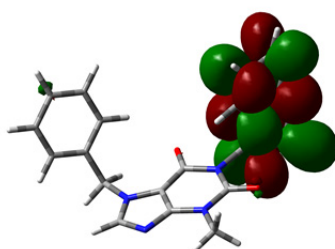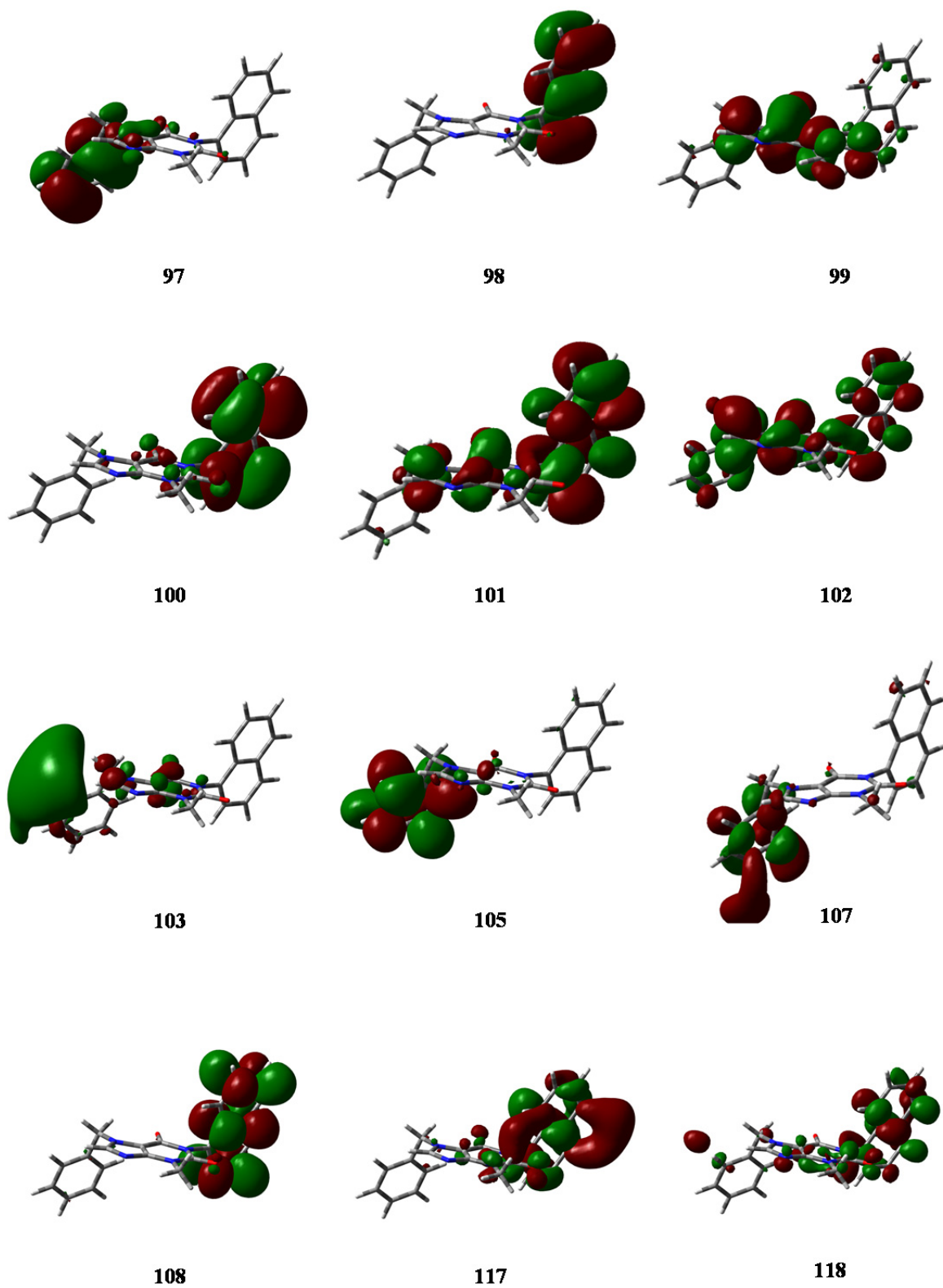
Figure 25 Calculated MOs of Compound 25c

The most populated MOs involved in the excitation state 3 at 259.4 nm show that the electron density is mainly present in the xanthine and naphthyl moieties, as shown in figure 25 for the *syn* and *anti* conformation.

The negative 270 nm band is due to the ^1L_a transitions[50] polarized along the short axis of the naphthalene chromophore.

Also in the case of wavelength of 208.74 nm and 208.83 nm, respectively for the *syn* and *anti* conformers, the most populated MOs involved in the excitation state 11 reveal that the electron density is mainly present in the xanthine and naphthyl moieties, as shown in figure 25 for the *syn* and *anti* conformation.

The positive 221 nm band is due to the ^1B_b transitions[6] polarized along the long axis of the naphthalene chromophore and the transitions polarized along the long axis of xanthine.

The dipoles coupling shown in figure below gives the positive dihedral angle P for both the *anti* and *syn* conformers.

GS-M-syn   GS-M-anti
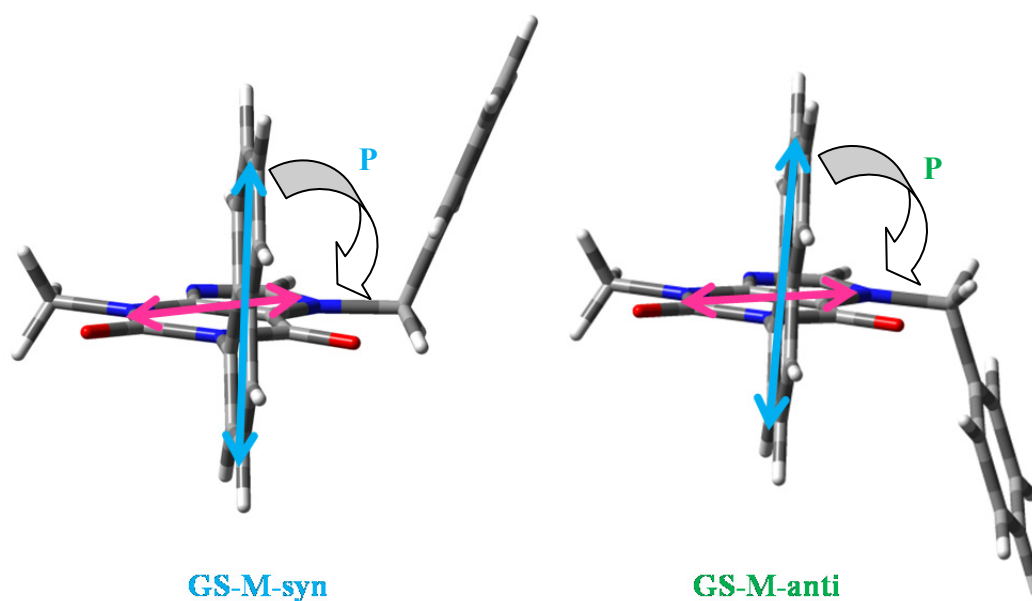
Figure 26 Band at 221 nm is given by the ^1B_b transitions along the long axis of naphthalene and the transitions on the long axis of xanthine

The band at 200 nm is the result of the three dipoles of naphthyl, xanthine and benzyl moiety and it is more complicated to report schematically.

Moreover, we have computed the ECD spectra with four different functionals (CAM-B3LYP, BH&HLYP, M06-2X, ωB97XD)[49] and all of them give the same bisignate final ECD curve

for the atropisomer M; therefore, comparing the calculated for the M atropisomer and the experimental of the second eluted peak, we can affirm that they are completely superimposable, leading us to conclude that the second eluted atropisomer has the M absolute configuration, while the first eluted peak is characterized by a clockwise dihedral angle about the chiral axis and it has P absolute configuration.
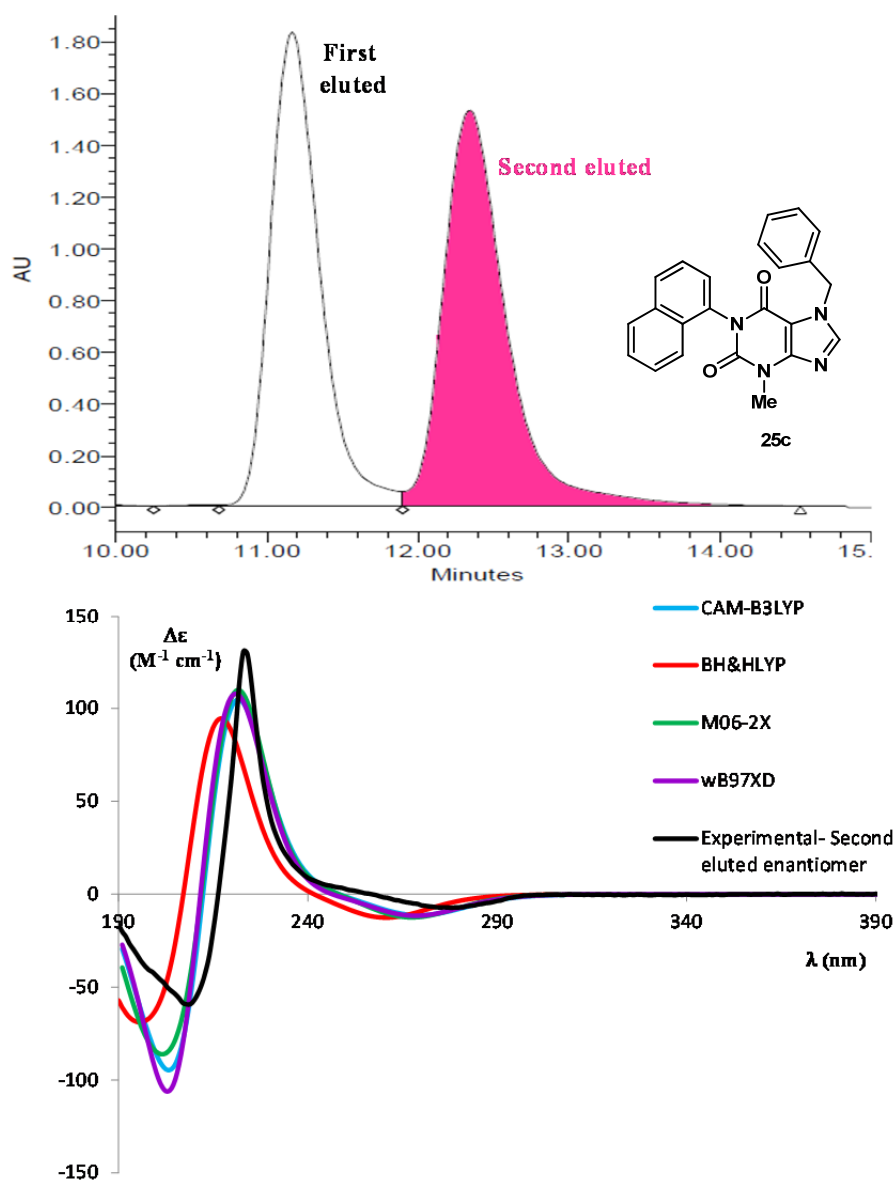
Figure 27 Compound 25c up: separation HPLC AD-H column; down: calculated final ECD spectrum of the M atropisomer compared to the experimental ECD spectrum of the second eluted enantiomer

As done for the configurational study for the naphthyl substituted xanthine, we have computed the ECD calculated spectra of enantiomer M of compound **25a** and **25b.** For these compounds we have to consider all of the four populated conformers as given by DFT ground state calculation (table 1).

The figure below shows both the experimental UV/Vis and ECD spectra of compound **25a**.

UV/Vis Spectrum
compound 25a

Experimental spectrum
first eluted enantiomer
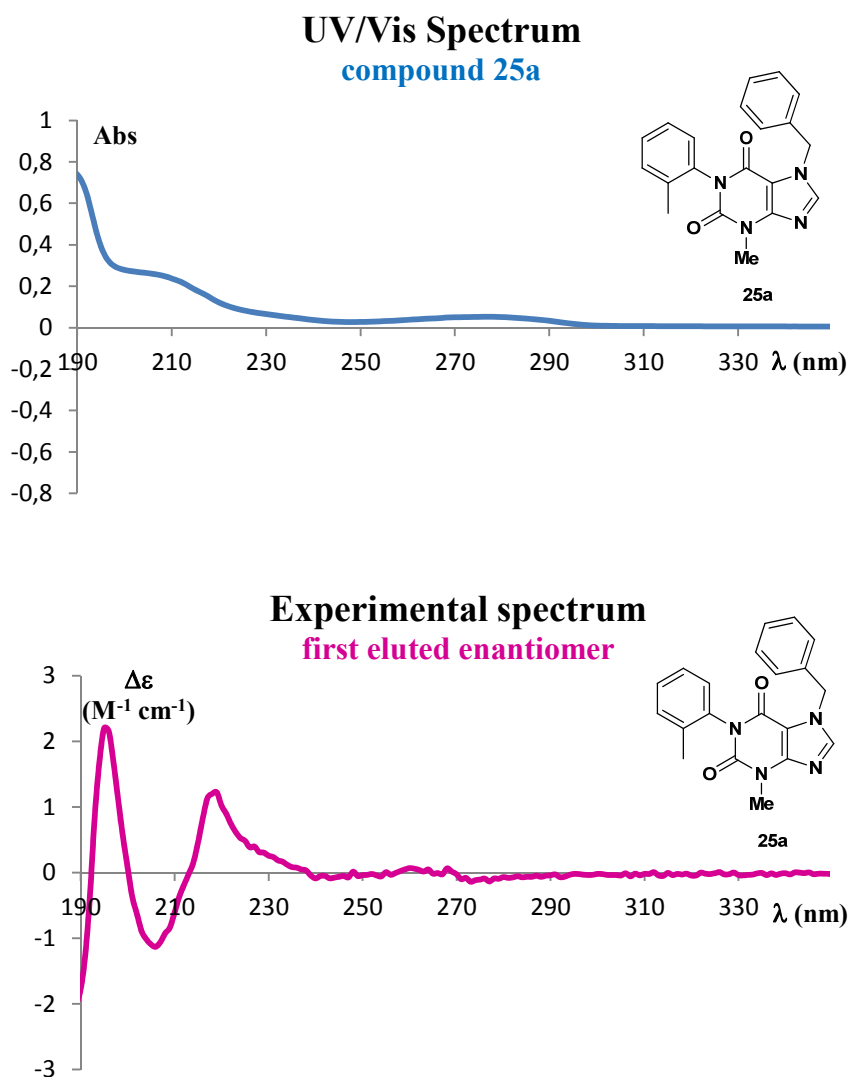
Figure 28 UV/Vis and ECD experimental spectra of compound **25a**

Looking at the simulated ECD spectra for the *anti* and *syn* conformations of the M atropisomer we found that they exhibit nearly opposite spectra (figure 29 of compound **25a**, see *Experimental procedure* for **25b**'s ECD spectra).
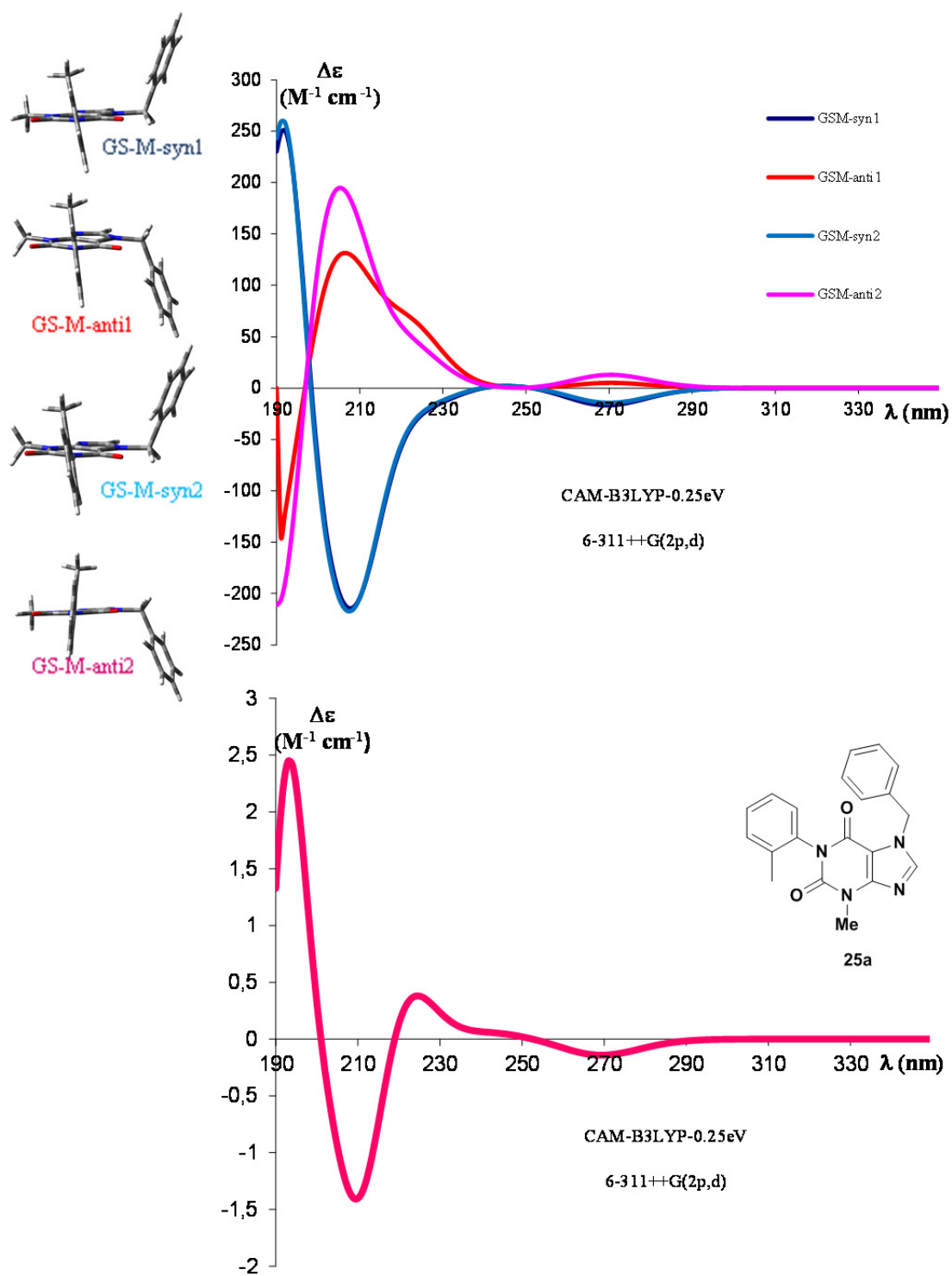
Figure 29 Compound 25a: computed ECD spectra for each populated GS conformations at the top; ECD calculated final spectrum at the bottom.

Since that the two conformations with different dihedral angle give the same spectra, the reasons for the inversion of the spectrum must be searched in the opposite disposition of the benzyl group with respect to the *ortho* substituent of the aryl ring in the two conformations. The combination of the two relative dispositions of the dipoles of benzyl produces opposite exciton coupling that leads to an inversion of the sign of the spectra depending on the side of the benzyl moiety.

For this reason the final calculated ECD spectrum of each atropisomeric compound is lowered because it is obtained by the weighted sum of the opposite contributions of all the possible conformations (figure 29).

To verify the robustness of the final computed ECD spectrum, that must be compared to the experimental spectrum to attribute the absolute configuration, we have obtained the simulated spectrum by modifying the conformational ratio from 90:10 to 10:90. As demonstrated by figure 30 the computed ECD spectrum is effectively robust, in particular we can notice that even at 90:10 and 10:90 the inversion of phase of the spectrum doesn't happen.
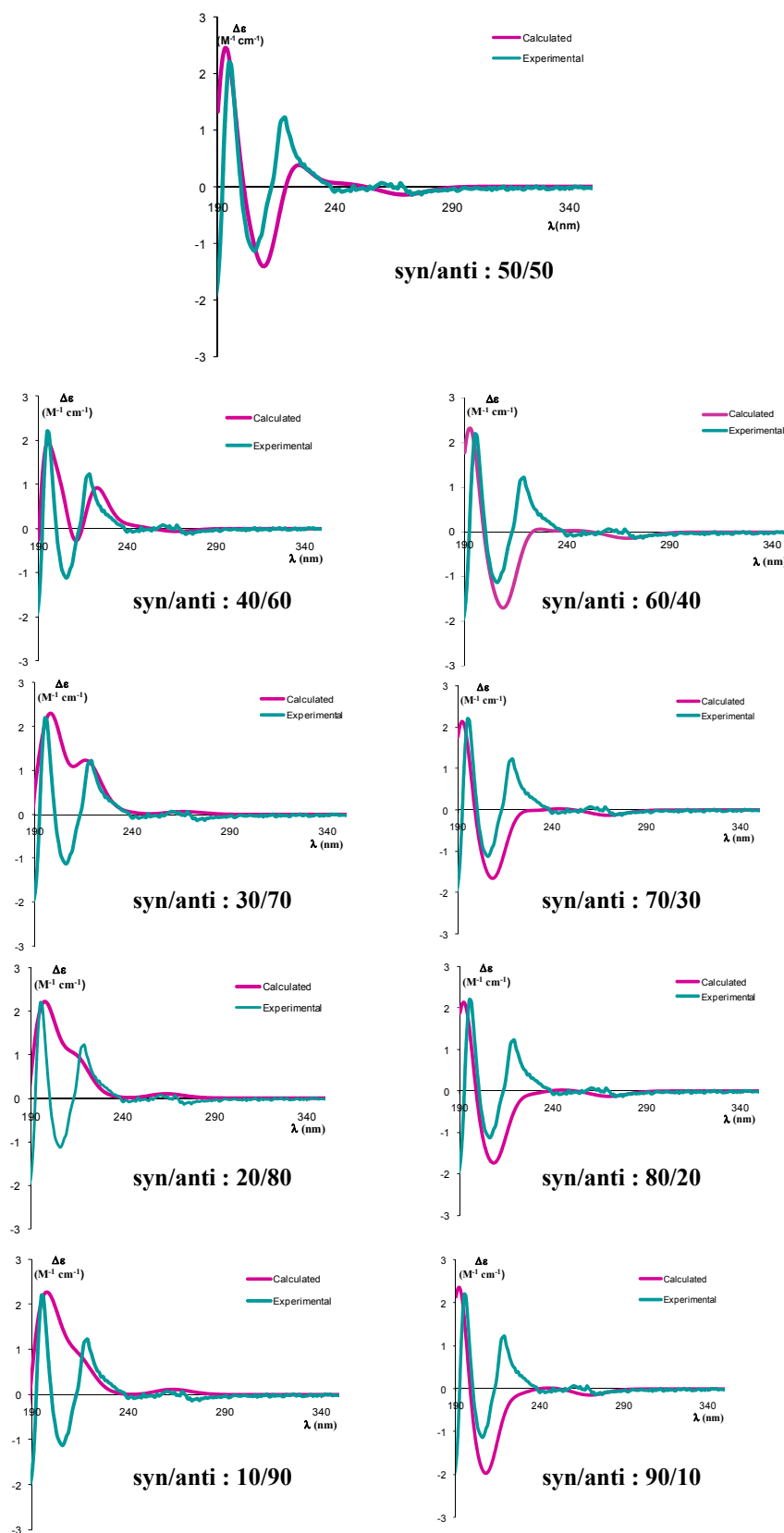
Figure 30 Calculated ECD spectra of compound 25a with different ratio *syn*:*anti* compared to the experimentally obtained.

The best matching of calculated and experimental data is given by a population ratio of about 50:50, as suggested by the relative energies calculated by DFT optimization. The experimental ECD spectra of **25a** and **25b** are showed in figure 31.
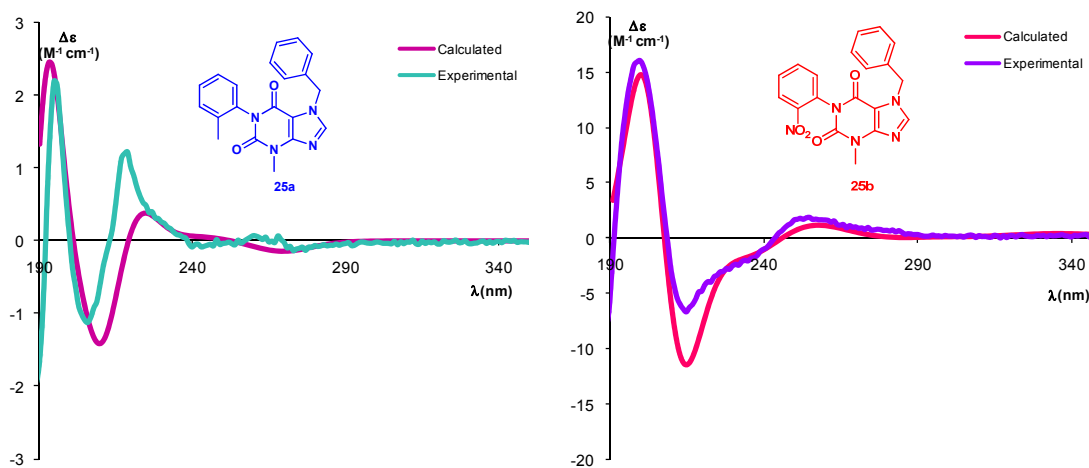
Figure 31 Experimental ECD spectra of first eluted atropisomer of compound 25a (left) and second eluted enantiomer of 25b (right).

The ECD bisignate curve of compound **25b** has a much weaker intensity respect to that of the naphthyl substituted xanthine. Also in this case three Cotton effects are present: the first at lower energies is positive and leads to a weak $\Delta\varepsilon$ maximum, while the other positive Cotton effect characterizes the higher energy band that is a more intense maximum. The only negative Cotton effect is attributable to the minimum at 217 nm. Compound **25a**, bearing the *o*-tolyl moiety, shows less intense absorption bands, because of the lack of a strong cromophore.

In conclusion, the comparison between the calculated and the experimental spectra leads us to attribute the absolute configuration to each atropisomeric structure of compounds **25a** and **25b**: the first eluted atropisomer bearing the *o*-tolyl substituent is the M atropisomer, while for compound **25b** we can affirm that the ECD calculated spectra for atropisomer M matches perfectly with that recorded experimentally for the second eluted peak. It should be noted that racemic **25b** was resolved on a cellulose-based HPLC column, while **25a** was resolved on an amilose-based column. The experimental outcomes suggests that the two columns have opposite selectivity for these compounds.

So keeping in mind that the two atropisomers of each xanthine derivative show opposite spectrum the table below shows all the absolute configuration attributed:

Table 7 Absolute configuration of the three xanthine derivatives

Entry	First eluted enantiomer	Second eluted enantiomer	Column
25a	M	P	AD-H
25b	P	M	Cellulose2
25c	P	M	AD-H

2.3 Future goals : diastereoisomeric xanthine derivatives

Since now we have investigated the newly created chiral axis $C(sp^2)$-N in position 1 of xanthine scaffold. Given that we have discovered that the naphthyl substituted purine base has the highest energy barrier of racemization, showing atropisomers stable at ambient temperature for 2353 years, we have decided to start from it to create a new chiral axis $C(sp^2)$-N in position 3 of the xanthine scaffold. The presence of another chiral axis will allow the formation of two diastereomeric pairs of xanthine derivative.

At first we have tried to investigate some coupling reactions linking to the N-3 a *metha* substituted aryl. Therefore, we focused our attention on the reactions that are shown below :
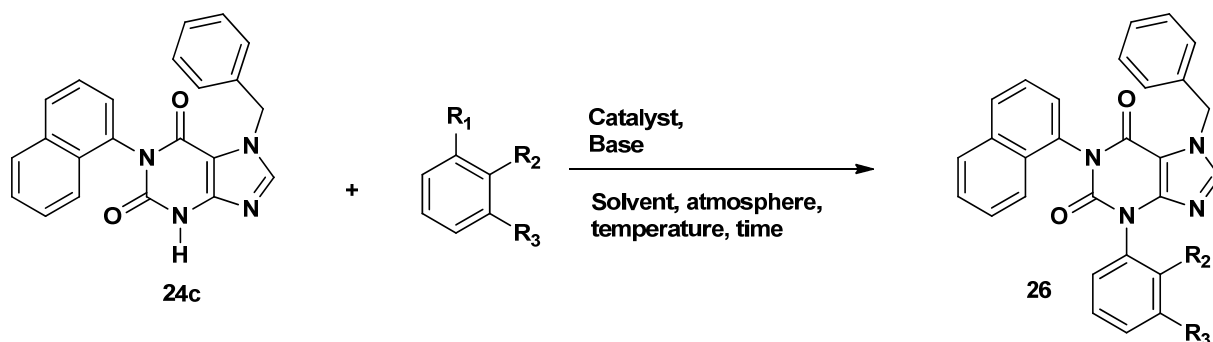
Figure 32 General synthetic scheme followed for the achieving of xanthine diastereoisomers

Table 8 Various reaction conditions for the achieving of xanthine diastereoisomers

Entry	R_1	R_2	R_3	Catalyst	Base	Solvent	Atmosphere	Temperature	Time	Yield
I	B(OH)$_2$	H	CH$_3$	Cu(OAc)$_2$[a]	NEt$_3$	CH$_2$Cl$_2$	O$_2$, 4 Å m.s.	r.t. → +40 °C	20 h	80%
II	B(OH)$_2$	H	CH$_3$	Cu(OAc)$_2$[a]	(-) Sparteine	CH$_2$Cl$_2$	O$_2$, 4 Å m.s.	r.t.	18 h	< 5%
III	B(OH)$_2$	H	CH$_2$CH$_3$	Cu(OAc)$_2$[a]	NEt$_3$	CH$_2$Cl$_2$	O$_2$, 4 Å m.s.	r.t. → +40 °C	20 h	70%
IV	Br	H	CH$_3$	Pd(OAc)$_2$[b] Xantphos (Pd/L=1/1.5)	Cs$_2$CO$_3$	DMF	N$_2$	+100 °C	1 h	< 5%
V	Br	CH$_3$	H	Pd$_2$(dba)$_3$[c] Xantphos (Pd/L=1/3)	Cs$_2$CO$_3$	1,4-dioxane	N$_2$	+100 °C.	12 h	0%
VI	B(OH)$_2$	NO$_2$	H	Cu(Cl)$_2$[d]	Net$_3$	DMSO	O$_2$, 4 Å m.s.	+100 °C	14 h	0%

[a] *The coupling reactions involving Copper as catalyst were conducted with: 1 eq. of 24c, 3 eq. of Boronic acid, 3 eq. of Cu(OAc)$_2$, 3 eq. of base.*

[b] *The coupling reaction involving Palladium as catalyst was conducted with:1.2 eq. of 24c, 1 eq. of Bromide, 10mol% of Pd(OAc)$_2$, 1.4 eq. of base.*

[c] *The coupling reaction involving Palladium as catalyst was conducted with:1 eq. of 24c, 1 eq. of Bromide, 0.005 eq. of Pd$_2$(dba)$_3$, 1.4 eq. of base.*

[d] *The coupling reaction involving Copper as catalyst was conducted with: 1 eq. of 24c, 1 eq. of Boronic acid, 1 eq. of CuCl$_2$, 1 eq. of base.*

As we can see in the table above, only the first and third reactions gave good results. Both of them are characterized by the same synthetic scheme of Chan-Lam coupling. For this reason, we decided to follow this reaction scheme coupling an *ortho*-methyl phenyl moiety to the N in position 3, to obtain stable atropisomers, rising the rotational energy barrier values. The only change made is the time of reaction that we increase from 20 h to 72 h.

Unfortunately we haven't obtained the *ortho* substituted product with the Chan Lam coupling, maybe because of the hindrance of the *ortho*-aryl boronic acid that during the catalytic cycle doesn't undergoes the reductive elimination step.

Recently, a new approach regarding the N-arylation of secondary amides has been published.[51] It allows the introduction of sterically hindered aryl groups under mild conditions. The new approach is based on metal-free N-arylation with diaryliodonium salts. Few attempts were done with purine **24c** and a first good result was obtained.
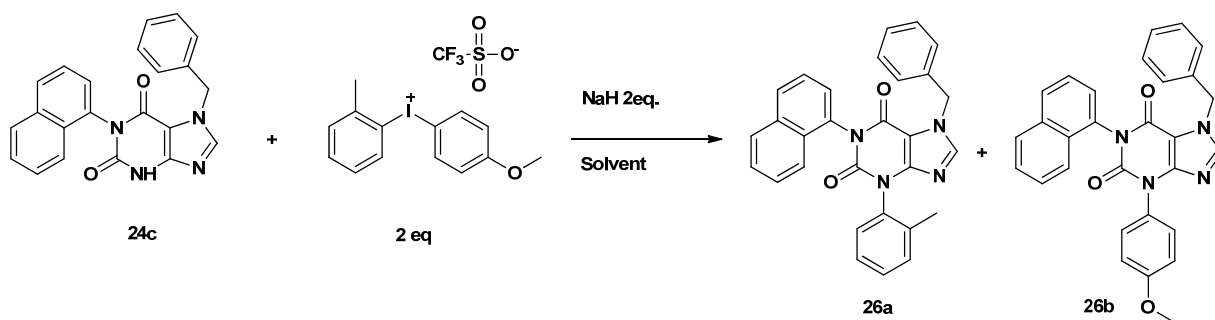
Figure 33 Synthetic scheme followed for the achieving of compound 26a

Table 9 Different reaction conditions for the synthesis of compound 26a

Entry	Solvent	Temperature	Yield (%)
1	Toluene	r.t.	0
2	THF	r.t.	0
3	THF	+66 °C	0
4	DMF	+100 °C	Product **26a**: 9 Product **26b**: 12

As shown in table only with DMF the reaction proceeded, giving the desired product **26a**.

The calculated energy barrier for this product is 23.5 kcal/mol, high enough to allow the separation of two diastereoisomers. A first separation test using the enantioselective AD-H column is shown by the chromatogram in figure 34. It displays the separation of stable atropisomers in ratio 22:28, referred to the first and third eluted respectively. The second eluted peak is the sum of the two other diastereoisomers.
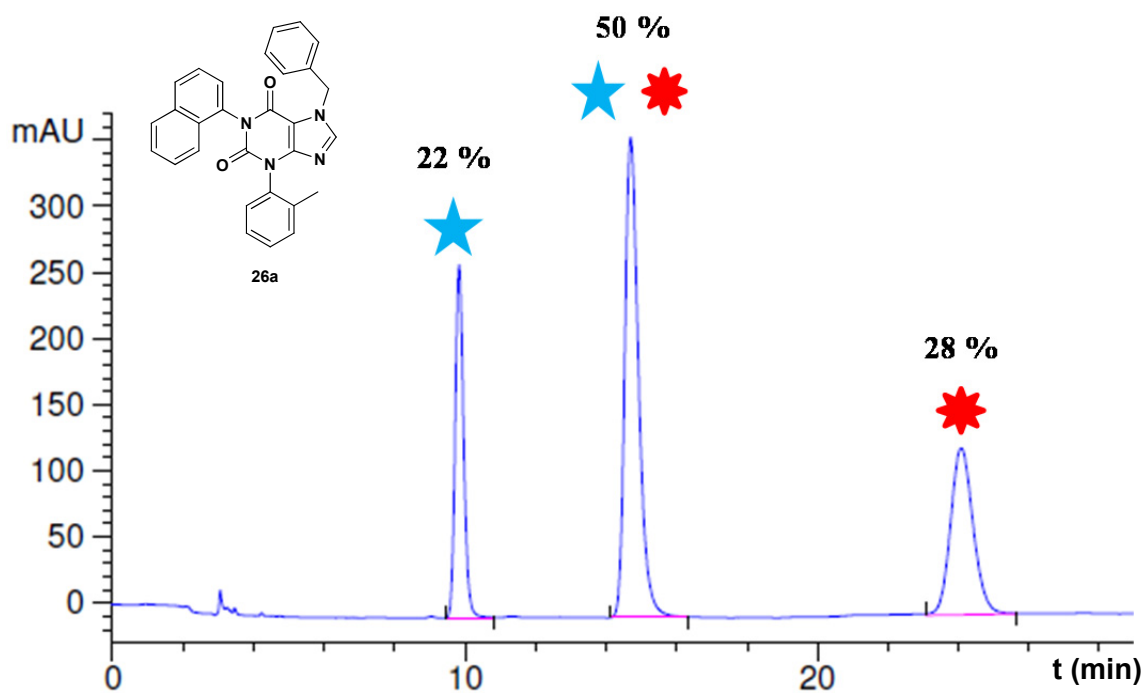
Figure 34 Enantiomeric separation of compound 26a by means of AD-H column

This could be a good starting point but there is still some way to go to study the stereodynamic of these new chiral compounds; first of all there is the necessity of improving the synthetic scheme, in order to get a variety of diasteromeric xanthine derivatives in good yields.

3. Conclusions

A new class of atropisomeric xanthine derivatives has been studied. We decided to focus our attention on these purine bases because of their various biological activities, that could play an important role in the discovery of new bioactive atropisomers.

The synthesized compounds **25a, 25b, 25c** are uncommon biaryl systems, but the newly created chiral axis in position 1 of the xanthine scaffold is a $C(sp^2)$-N axis, around which the rotation is prevented by the presence of bulky *ortho* substituents.

The conformational stability has been predicted by means of DFT simulations yielding a rotational energy barrier higher than 25 kcal/mol.

Through a retro synthetic analysis, we proceeded to the synthesis and characterization of the three structures.

The computed activation energy values were compared to the experimental data that have been obtained by means of kinetic studies, following the thermal racemization process with an enantioselective HPLC. As expected the increasing of bulkiness of the *ortho* position of the aryl moiety caused a rising of the rotational energy barrier; while, surprisingly, compound **25b**, bearing a *o*-nitro phenyl group in position 1, showed a lower activation energy respect to that characterizing compound **25a** that has a *o*-tolyl substituent. A possible explanation is that even if the methyl and nitro group are isosteric, the second develops electronic interactions with the carbonyl groups of the xanthine scaffold, thus stabilizing the transition state and lowering the energy barrier.

Once determined the interconversion energy barrier values of all the derivatives, we have calculated the half- life time both at ambient temperature and at +37 °C (the normal human body temperature), which is an important parameter to consider when a bioactive atropisomeric molecule is developed in the field of drug discovery. From these results we can affirm that compound **25a** and **25b** belong to the Class 2 of LaPlante classification scheme, while **25c** is more stable and can be described as a LaPlante's Class 3 compound (compound 25a: $\Delta G^{\neq}$= 30.47 kcal/mol; compound 25b: $\Delta G^{\neq}$= 25.37 kcal/mol; compound 25c: $\Delta G^{\neq}$= 32.50 kcal/mol).

The absolute configuration was finally assigned using the ECD technique. Compound **25c** showed an experimental ECD spectrum characterized by intense bands due to the presence of exciton coupling between the transition moments of chromophores of the atropisomeric molecule. The electronic transitions that generated the CD bisignate curve have been also studied by analyzing the the MOs involved.

Looking at the simulated ECD spectra of compounds **25a** and **25b** for the *anti* and *syn* conformations of the M atropisomer we found that they exhibit nearly opposite spectra. Since that the two conformations with different dihedral angle give the same spectra, the combination of the two relative dispositions of the dipoles of benzyl produces opposite exciton coupling that leads to an inversion of the sign of the spectra depending on the side of the benzyl moiety. After verifying the robustness of the final computed ECD spectrum tuning the population ratio of *syn*/*anti* conformations, we compared the calculated ECD spectrum to the experimentally obtained of a pure enantiomeric form.

From the matching of the two spectra we were able to assign the absolute configuration of each atropisomeric structure.

Table 10 Absolute configuration of the three xanthine derivatives

Entry	First eluted enantiomer	Second eluted enantiomer	Column
25a	M	P	AD-H
25b	P	M	Cellulose2
25c	P	M	AD-H

Given that we have discovered that the naphthyl substituted purine base has the highest energy barrier of racemization, the future goals would be to create diasteromeric xanthine derivatives starting from it and making a new $C(sp^2)$-N chiral axis in position 3 of the xanthine molecule. We screened some coupling reactions and we found that a metal-free coupling, involving iodonium salts can yield the desired compounds.

It would be also interesting to explore the biological activity of the atropisomeric xanthines synthesized because of their potential pharmacological interest.

4. Experimental section

4.1 Materials

Cyanamide, triethyl orthoformate, ethyl 2-bromoacetate and phenylmethanamine were commercially available. Cyanamide was purified washing with acetonitrile to eliminate the water and then dried. Triethyl orthoformate was distilled before use. THF has been dried before use by distillation from Na/benzophenone. The deuterated solvents for NMR spectra were commercially available.

4.2 Instrumentations

The following stationary phases were employed for the chromatography: Silica gel 60 F254 (Merck) for the TLC and silica gel 60 Å (230-400 mesh, Sigma Aldrich) for atmospheric pressure chromatography.

Reactions which needed anhydrous conditions were performed under dried nitrogen flow (inert atmosphere). The glassware used in these reactions was placed in an oven at +70 °C for at least 3 hours immediately before use.

To purify the products, a HPLC Waters^{TM} 600 instrument with detection fixed at 254 nm was used. Phenomenex Luna C18 (5 μm 250x21.2 mm, 20 mL/min) semipreparative column was used to purify the compounds using mixtures of acetonitrile and water as eluents.

Enantioselective HPLC columns (DAICEL Chiralcel AD-H 5μm 250 × 21.2 mm, 20 mL/min; Phenomenex Lux Cellulose-2 5μm, 250 x 10 mm, 5mL/min) have been used to separate the stable atropisomers, using different mixtures of hexane and isopropanol as eluent.

^{1}H-NMR, and ^{13}C-NMR spectra were registered with a Varian Inova 600 MHz and a Varian Mercury 400 MHz spectrometer. Chemical shifts are given in ppm relative to the internal standards tetramethylsilane (^{1}H and ^{13}C) or relative to the residual peak of the solvents. Assignment of the carbons multiplicity were obtained by means of the DEPT sequences.

ECD spectra were recorded with a JASCO J-810 spectropolarimeter at +25 °C in acetonitrile solutions. The concentrations of the samples were tuned to obtain a maximum absorbance of about 0.9-1.0 in the UV spectrum, using a quartz cell with 0.2 cm path length.

4.3 Calculations

A conformational search was preliminarily carried out by means of the molecular mechanics force field (MMFF), using the package ComputeVOA 0.1.[52] The most stable conformers thus identified were subsequently energy minimized by DFT computations, which were performed by the Gaussian 09, rev. D.01, series of programs using standard optimization parameters.[53] The calculations for ground states and transition states employed the B3LYP hybrid HF-DFT method and the 6-31G(d) basis sets. The analysis of the vibrational frequencies for every optimized structure has shown the absence of imaginary harmonic frequencies for the ground states, and the presence of a single imaginary frequency for the transition states. Visual inspection of the corresponding normal mode[54] validated the identification of the transition states.

The ECD spectra were simulated by means of TD-DFT calculations. The electronic excitation energies and rotational strengths have been calculated in the gas phase using the geometries obtained at the B3LYP/6-31G(d) level with the CAM-B3LYP functional. All the calculations employed the 6-311++G(2d,p) basis set because this basis set has been widely used in this kind of calculation and proved to be sufficiently accurate at a reasonable computational cost. The simulated spectra were obtained using the first 60 calculated transitions (lowest wavelength about 180 nm) and applying a 0.25 eV line width. The simulated spectra resulting from the Boltzmann averaged sum of the conformations were red-shifted by 10 nm to get the best simulations with the experimental spectra.

4.4 Synthesis

4.4.1 General procedure

Through a retrosynthetic analysis[55] the three xanthines were prepared following the general synthetic scheme reported below:
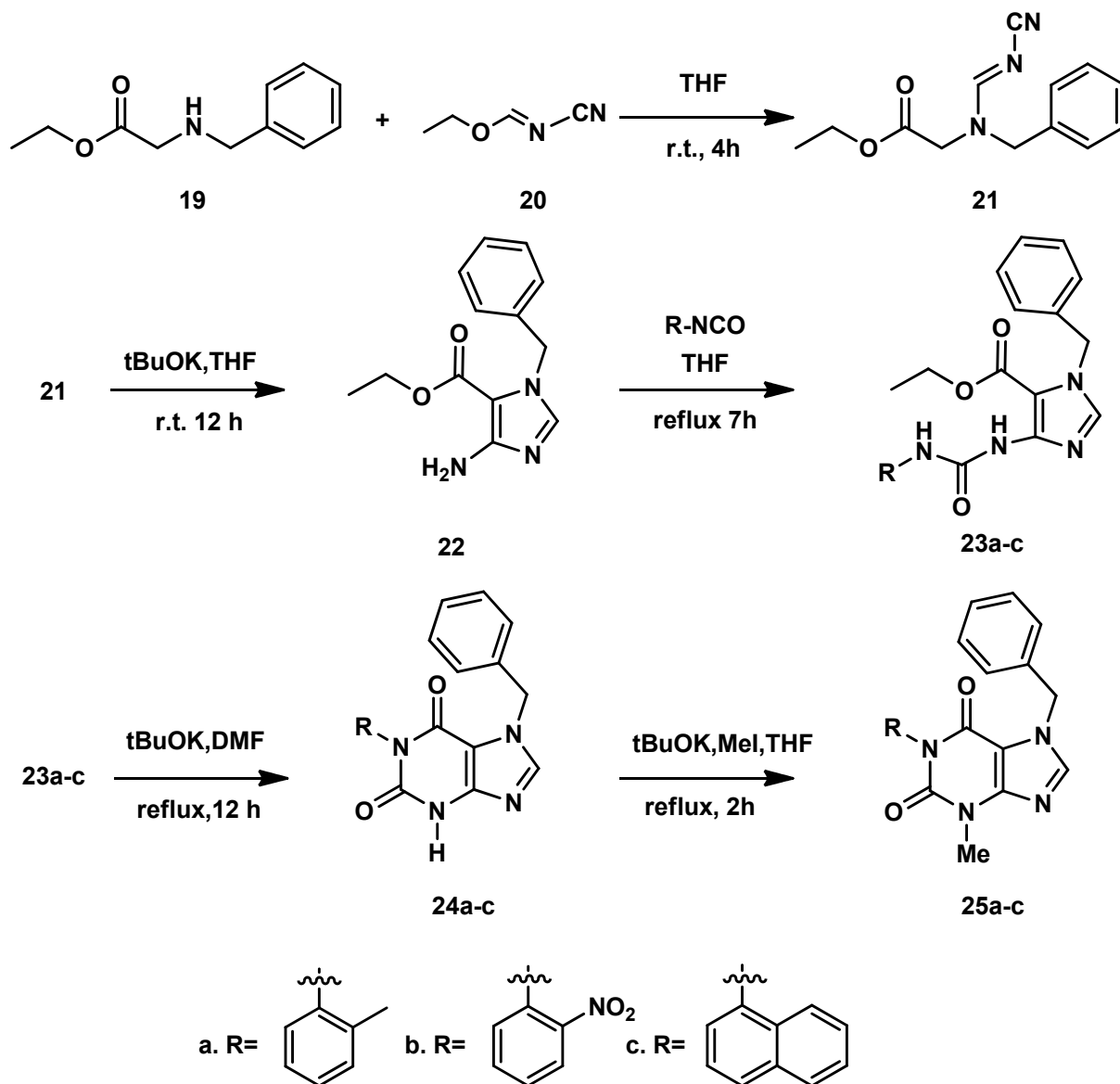
Figure 34 General synthetic procedure

The two starting reagents were produced from commercially available products using the synthetic scheme reported:
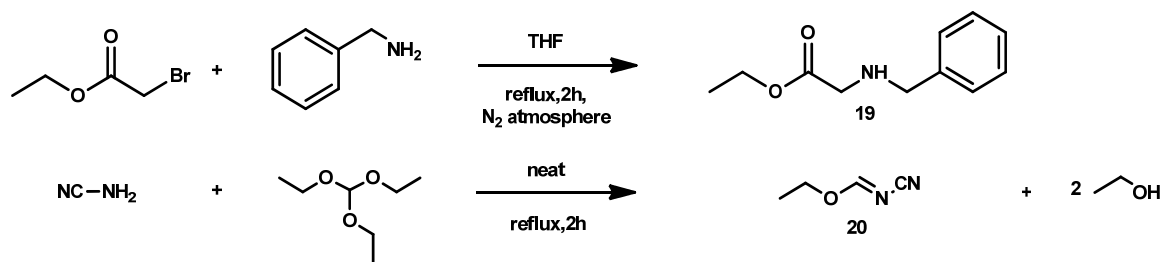
Figure 35 Synthesis of the two starting compounds

4.4.2 Synthesis of the two starting compounds

Ethyl 2-(benzylamino)acetate (19):
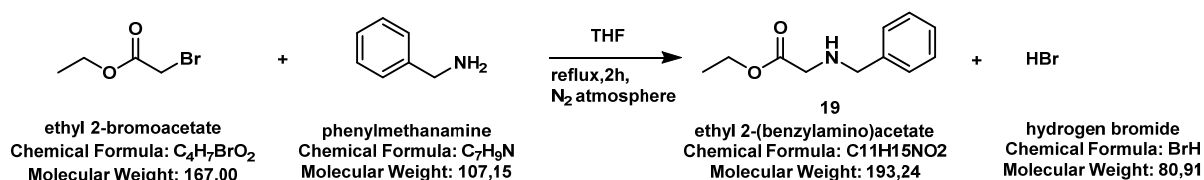
Ethyl 2-bromoacetate (11.09 mL, 0.1 mol) was dissolved in dry THF (100 mL) and the solution was cooled in an ice-water bath. Phenylmethanamine (21.84 mL, 0.2 mol) was diluted in dry THF (100 mL) and the solution was added to ethyl 2-bromoacetate dropwise. After the addition the ice bath was removed, and the reaction mixture was stirred under reflux for 2 h under nitrogen atmosphere. This mixture was quenched with an aqueous solution of NaOH and extracted with CH_2Cl_2. The combined organic layer was dried with Na_2SO_4, filtered, concentrated under reduced pressure and purified by fractional distillation under vacuum conditions (ethyl 2-(benzylamino)acetate: b.p. +110 °C / 2 mbar. The product was obtained as a colorless liquid with a yield of 76% (14.69 g).

Spettroscopic data:

^{1}H-NMR (400 MHz, CDCl$_3$, TMS, +25 °C): δ 1.27 (t, J=7.2 Hz, 3H); 1.87 (s, NH); 3.41 (s, 2H); 3.81 (s, 2H); 4.20 (q, J=7.2, 2H); 7.26-7.33 (m, 5H).

^{13}C-NMR (100.6 MHz, CDCl$_3$, 77.0 ppm, +25 °C): δ 14.2 (CH$_3$); 50.1 (CH$_2$); 53.3 (CH$_2$); 60.7 (CH$_2$); 127.1 (CH); 128.2 (2CH); 128.4 (2CH); 139.5 (Cq); 172.4 (Cq).

Ethyl-N-cyanoformimidate (20)

cyanamide
Chemical Formula: CH_2N_2
Molecular Weight: 42,04

triethoxymethane
Chemical Formula: $C7H16O3$
Molecular Weight: 148,20

ethyl N-cyanoformimidate
Chemical Formula: $C4H6N2O$
Molecular Weight: 98,10

ethanol
Chemical Formula: $C2H6O$
Molecular Weight: 46,07
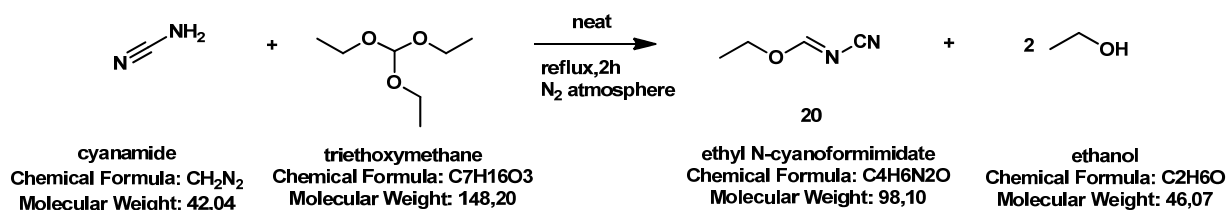
Cyanamide (12.73 g, 0.303 mol) was dissolved in triethyl orthoformate (d= 0.891g/mL, 40 mL, 0.303 mol) and the solution was heated under reflux for 2 h under nitrogen atmosphere, then the EtOH was removed by distillation (b.p. +78 °C). Fractional distillation under vacuum conditions of the residue gave ethyl N-cyanoformimidate (yield 80%) with b.p. +80 °C / 5 mbar. Before distilling the desired product we removed the remaining triethyl orthoformate and the side-product ethyl formate formed during the reaction by means of distillation (ethyl-formate b.p. +54°C; triethyl orthoformate b.p. +56 °C/37 mbar).

Spectroscopic data

^{1}H-NMR (400 MHz, CDCl_3, TMS, +25 °C): δ 1.40 (t, J=7.2 Hz, 3H); 4.39 (q, J=7.2 Hz, 2H); 8.41 (s, 1H).

^{13}C-NMR (100.6 MHz, CDCl_3, 77 ppm, +25 °C): δ 13.5 (CH_3); 65.8 (CH_2); 113.6 (Cq); 171.2 (CH).

4.4.3 Synthesis of ethyl 4-amino-1-benzyl-1H-imidazole-5-carboxylate (22)

19
ethyl 2-(benzylamino)acetate
Chemical Formula: $C_{11}H_{15}NO_2$
Molecular Weight: 193,24

20
ethyl N-cyanoformimidate
Chemical Formula: $C_4H_6N_2O$
Molecular Weight: 98,10

21
ethyl 2-(N-benzyl-N'-cyanoformimidamido)acetate
Chemical Formula: $C_{13}H_{15}N_3O_2$
Molecular Weight: 245,28

22
ethyl 4-amino-1-benzyl-1H-imidazole-5-carboxylate
Chemical Formula: $C_{13}H_{15}N_3O_2$
Molecular Weight: 245,28
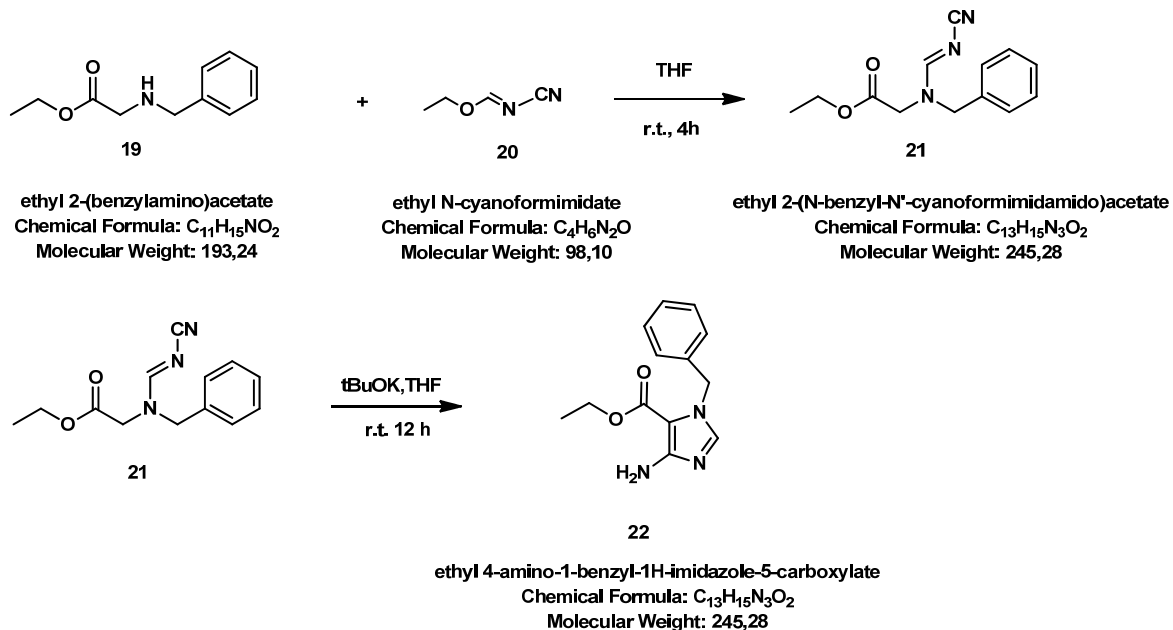
Two steps synthesis

First Step (21)

Ethyl-2-(benzilamino)acetate (3.00 g, 15.52 mmol) in THF (75 mL) was cooled in an ice-water bath, and ethyl N-cyanoformimidate (1.523 g, 15.52 mmol) in 38 mL of THF was added dropwise. The reaction mixture was stirred at room temperature for 4 h. The mixture was concentrated under reduced pressure and was passed through a silica gel plug (EtOAc:Hexane = 30:70 with gradient to 100:0) to remove impurities. The intermediate appeared as a pale yellow liquid and was obtained with a yield of 97% (3.693 g).

Second Step (22)

t-BuOK (1.742 g, 31.04 mmol) was added to intermediate **21** in 137 mL of THF and the reaction mixture was stirred over night at room temperature. The mixture was quenched with 100 mL of an aqueous solution of NH_4Cl and extracted with CH_2Cl_2. The combined organic layer was dried with Na_2SO_4, filtered, concentrated under reduced pressure and purified by column chromatography (EtOAc : Hexane = 2:1 with gradient to 1:0). After recrystallization from Et_2O, the product was obtained with a 60% yield (2.215 g) as a colorless solid.

Spectroscopic data

COMPOUND 21

^{1}H-NMR (400 MHz, CDCl$_3$, TMS, +25 °C): E+Z stereoisomers δ 1.23-1.29 (m,6H); 3.92 (s, 1H); 4.04 (s,1H); 4.17-4.23 (m,4H); 4.58 (s,2H); 4.69 (s,2H); 7.21-7.44 (m, 10H); 8.21 (s,1H); 8.30 (s, 1H).

^{13}C-NMR (150.8 MHz, CDCl$_3$, 77 ppm, +25 °C): δ 14.03 (CH$_3$); 14.05 (CH$_3$); 46.0 (CH$_2$); 49.7 (CH$_2$); 51.4 (CH$_2$); 56.5 (CH$_2$); 61.9 (CH$_2$); 62.2 (CH$_2$); 117.5 (Cq); 117.87 (Cq); 128.2 (CH); 128.6 (CH); 128.7 (CH); 128.9 (CH); 129.1 (CH); 129.3 (CH); 133.0 (Cq); 133.5 (Cq); 164.2 (CH); 165.2 (CH); 166.8 (Cq); 167.5 (Cq).

COMPOUND 22

^{1}H-NMR (400 MHz, CDCl$_3$, TMS, +25 °C): δ 1.25 (t, *J*=7.2 Hz, 3H); 4.24 (q, *J*=7.2 Hz, 2H); 4.87(NH$_2$); 5.34 (s, 2H); 7.14 (d, *J*= 6.70 Hz, 2H); 7.23 (s,1H); 7.27-7.35 (m, 3H).

^{13}C-NMR (150.8 MHz, CDCl$_3$, 77 ppm, +25 °C): δ 14.5 (CH$_3$); 50.7 (CH$_2$); 59.7 (CH$_2$); 102.0 (Cq); 126.9 (CH); 127.8 (CH); 128.8 (CH); 136.7 (Cq); 139.3 (CH); 161.02 (Cq).

4.4.4 Synthesis of 7-benzyl-3-methyl-1-(o-tolyl)-1H-purine-2,6(3H,7H)-dione (25a)

22
ethyl 4-amino-1-benzyl-1H-imidazole-5-carboxylate
Chemical Formula: $C_{13}H_{15}N_3O_2$
Molecular Weight: 245,28

1-isocyanato-2-methylbenzene
Chemical Formula: C_8H_7NO
Molecular Weight: 133,15

24a
7-benzyl-1-(o-tolyl)-1H-purine-2,6(3H,7H)-dione
Chemical Formula: $C_{19}H_{16}N_4O_2$
Molecular Weight: 332,36

24a
7-benzyl-1-(o-tolyl)-1H-purine-2,6(3H,7H)-dione
Chemical Formula: $C_{19}H_{16}N_4O_2$
Molecular Weight: 332,36

25a
7-benzyl-3-methyl-1-(o-tolyl)-1H-purine-2,6(3H,7H)-dione
Chemical Formula: $C_{20}H_{18}N_4O_2$
Molecular Weight: 346,38

Two steps synthesis

First Step (24a)

o-Tolyl isocyanate (0.05 mL, 0.4 mmol) was added to a solution of **22** (0.050 g, 0.2 mmol) in THF (4.7 mL) and the reaction mixture was stirred under reflux conditions for 7h. The resulting mixture was concentrated under reduced pressure conditions yielding product **23a**. DMF and t-BuOK (0.067g, 0.6mmol) were added to **23a**. The mixture was stirred under reflux overnight. Subsequently, the mixture was quenched with an aqueous solution of HCl and extracted with EtOAc. The combined organic layer was dried with Na_2SO_4, filtered, concentrated under reduced pressure and purified by column chromatography (EtOAc : Hexane = 2:1 with gradient to 1:0) to afford product **24a** with a 80% yield (0.053 g).

Second Step (25a)

Product **24a** was dissolved in THF and t-BuOK (0.036g, 0.32mmol) followed by MeI (d= 2.28 g/mL, 0.02 mL, 0.32 mmol) were added. The mixture was stirred under reflux conditions for 2h and after that, it was extracted with EtOAc. The combined organic layer was dried with Na_2SO_4, filtered and concentrated under reduced pressure to give the compound **25a** with 98% yield (0.054 g).

COMPOUND 24A

^{1}HNMR (600 MHz, CD$_3$CN, +25 °C): δ 2.07 (s, 3H); 5.46 (s, 2H); 7.15 (d, *J*=7.8 Hz, 1H); 7.29-7.38 (m, 8H); 7.85 (s,1H);9.87 (NH).

^{13}CNMR (150.8 MHz, CD$_3$CN, 1.79 ppm, +25 °C): δ 16.6 (CH$_3$); 49.6 (CH$_2$); 106.9 (Cq); 126.8 (CH); 127.8 (CH); 128.2 (CH); 128.8 (CH); 128.9 (CH); 129.4 (CH); 130.7 (CH); 135.3 (Cq); 136.8 (Cq); 136.9 (Cq); 142.5 (CH); 148.4 (Cq); 150.9 (Cq); 155.3(Cq).

COMPOUND25A

^{1}HNMR (600 MHz, CD$_3$CN, +25 °C): δ 2.06 (s, 3H); 3.51 (s, 3H); 5.48 (s, 2H); 7.13 (d, *J*=7.8 Hz, 1H); 7.30-7.37 (m, 8H); 7.89 (s,1H).

^{13}CNMR (150.8 MHz, CD$_3$CN, 1.79 ppm, +25 °C): δ 17.4 (CH$_3$); 30.1 (CH$_3$); 50.6 (CH$_2$); 107.8 (Cq); 127.6 (CH); 128.7 (CH); 129.1 (CH); 129.5 (CH); 129.7 (CH); 130.2 (CH); 131.5 (CH); 136.7 (Cq); 137.6 (Cq); 137.8 (Cq); 143.1 (CH); 150.9 (Cq); 152.1 (Cq); 155.6(Cq).

4.4.5 Synthesis of 7-benzyl-3-methyl-1-(2-nitrophenyl)-1H-purine-2,6(3H,7H)-dione (25b)

22
ethyl 4-amino-1-benzyl-1H-imidazole-5-carboxylate
Chemical Formula: C$_{13}$H$_{15}$N$_3$O$_2$
Molecular Weight: 245,28

1-isocyanato-2-nitrobenzene
Chemical Formula: C$_7$H$_4$N$_2$O$_3$
Molecular Weight: 164,12

7-benzyl-1-(2-nitrophenyl)-1H-purine-2,6(3H,7H)-dione
Chemical Formula: C$_{18}$H$_{13}$N$_5$O$_4$
Molecular Weight: 363,33

24b
7-benzyl-1-(2-nitrophenyl)-1H-purine-2,6(3H,7H)-dione
Chemical Formula: C$_{18}$H$_{13}$N$_5$O$_4$
Molecular Weight: 363,33

25b
7-benzyl-3-methyl-1-(2-nitrophenyl)-1H-purine-2,6(3H,7H)-dione
Chemical Formula: C$_{19}$H$_{15}$N$_5$O$_4$
Molecular Weight: 377,35

Two steps synthesis

First Step (24b)

o-Nitro-phenylisocyanate (0.131g, 0.8 mmol) was added to a solution of **22** (0.050 g, 0.2 mmol) in THF (4.7 mL) and the reaction mixture was stirred under reflux conditions for 7h. The resulting mixture was concentrated under reduced pressure conditions and compound **23b** was obtained. DMF and t-BuOK (0.064g, 0.57mmol) were added to **23b**. The mixture was stirred under reflux overnight. Subsequently, the mixture was quenched with an aqueous solution of HCl and extracted with EtOAc. The combined organic layer was dried with Na_2SO_4, filtered, concentrated under reduced pressure and purified by semipreparative HPLC on a Luna C18 column (10 μm, 250 x 21.2 mm, 25 mL/min, $ACN:H_2O$ = 63:37 v/v) to afford product **24b** with a 65% yield (0.047 g).

Second Step (25b)

Product **24b** was dissolved in THF and t-BuOK (0.028 g, 0.25 mmol) followed by MeI (d=2.28 g/mL, 0.016 mL, 0.25 mmol) were added. The mixture was stirred under reflux conditions for 2h and after that, it was extracted with EtOAc. The combined organic layer was dried with Na_2SO_4, filtered and concentrated under reduced pressure to give the compound **25b** with 97% yield(0.048 g)

Spectroscopic data

COMPOUND 24B

¹H-NMR (600 MHz, CD_3CN, +25 °C): δ 5.42 (d, *J*= 15.2 Hz, 1H); 5.45 (d, *J*=15.2 Hz, 1H); 7.32-7.38 (m, 5H); 7.52 (dd, *J* =7.9, 1.5 Hz, 1H); 7.69 (ddd, *J*=8.2, 7.6, 1.5 Hz, 1H); 7.84 (ddd, *J*=7.9, 7.6, 1.5 Hz, 1H); 7.9 (s, 1H); 8.16 (dd, *J*=8.2, 1.5 Hz, 1H); 9.52 (NH).

¹³C-NMR (150.8 MHz, CD_3CN, 1.79 ppm, +25 °C) : δ 50.6 (CH_2); 107.6 (Cq); 126.2 (CH); 128.6 (CH); 129.2 (CH); 129.8 (CH); 130.4 (Cq); 130.9 (CH); 133.2 (CH); 135.4 (CH); 137.5 (Cq); 144.0 (CH); 147.7 (Cq); 149.6 (Cq); 151.4 (Cq); 155.8 (Cq).

COMPOUND 25B

¹HNMR (600 MHz, CD_3CN,+25 °C): δ 3.52 (s, 3H); 5.45 (d, *J*= 15.4 Hz, 2H); 5.47 (d, *J*= 15.4 Hz, 2H); 7.32-7.38 (m, 5H); 7.49 (dd, *J*=8.0, 1.4 Hz, 1H); 7.70 (td, *J*=8.1, 1.4 Hz, 1H); 7.84(td, *J*=7.7, 1.5 Hz,1H); 7.93(s,1H); 8.16 (dd, *J*=8.2, 1.6 Hz, 1H).

13CNMR (150.8 MHz, CD$_3$CN,1.79 ppm, +25 °C) : δ 29.2 (CH$_3$); 49.8 (CH$_2$); 106.7 (Cq); 125.3 (CH); 127.7 (CH); 128.2 (CH); 128.8 (CH); 129.9 (Cq); 130.0 (CH); 132.2 (CH); 134.4 (CH); 136.5 (Cq); 142.7 (CH); 146.7 (Cq); 150.2 (Cq); 150.9 (Cq); 154.3 (Cq).

4.4.6 Synthesis of 7-benzyl-3-methyl-1-(naphthalen-1-yl)-1H-purine-2,6(3H,7H)-dione (25c)

ethyl 4-amino-1-benzyl-1H-imidazole-5-carboxylate
Chemical Formula: C13H15N3O2
Molecular Weight: 245,28

1-isocyanatonaphthalene
Chemical Formula: C11H7NO
Molecular Weight: 169,18

7-benzyl-1-(naphthalen-1-yl)-1H-purine-2,6(3H,7H)-dione
Chemical Formula: C22H16N4O2
Molecular Weight: 368,39

24c
7-benzyl-1-(naphthalen-1-yl)-1H-purine-2,6(3H,7H)-dione
Chemical Formula: C22H16N4O2
Molecular Weight: 368,39

25c
7-benzyl-3-methyl-1-(naphthalen-1-yl)-1H-purine-2,6(3H,7H)-dione
Chemical Formula: C23H18N4O2
Molecular Weight: 382,41

Two steps synthesis

First Step (24c)

1-Naphtyl-isocyanate (d= 1.177 g/mL, 0.575 mL, 4 mmol) was added to a solution of **22** (0.50g, 2mmol) in THF (47mL) and the reaction mixture was stirred under reflux conditions for 7h. The resulting mixture was concentrated under reduced pressure conditions and the product **23c** was obtained. DMF and t-BuOK (0.67 g, 6 mmol) were added to **23c**. The mixture was stirred under reflux overnight. Subsequently, the mixture was quenched with an aqueous solution of HCl and extracted with EtOAc. The combined organic layer was dried with Na_2SO_4, filtered, concentrated under reduced pressure and purified by semipreparative HPLC on a Luna C18 column (10 μm, 250 x 21.2 mm, 25 mL/min, ACN:$H_2$0 = 90:10 v/v) to afford product **24c** as a white solid with a 80% yield (0.589 g).

Second Step (25c)

Product **24c** was dissolved in THF and t-BuOK (0.036 g, 0.32 mmol) followed by MeI (d=2.28 g/mL, 0.02 mL, 0.32 mmol) were added. The mixture was stirred under reflux conditions for 2h and after that, it was extracted with EtOAc. The combined organic layer was

dried with Na$_2$SO$_4$, filtered and concentrated under reduced pressure to give the compound **25c** with 98% yield (0.600 g).

Spectroscopic data

COMPOUND 24c

^{1}H-NMR (600 MHz, CD$_3$CN, +25 °C): δ 5.46 (s, CH$_2$); 7.31-7.38 (m, 5H); 7.45 (d, *J*=7.4 Hz, 1H); 7.49-7.51 (m, 1H); 7.55-7.58 (m, 1H); 7.61-7.63 (m, 1H); 7.66 (d, *J*=8.2 Hz, 1H); 8.01 (dd, *J*=8.2, 2.4 Hz, 2H); 9.73 (NH).

^{13}C-NMR (150.8 MHz, CD$_3$CN, 1.79 ppm, +25 °C) : δ 51.0 (CH$_2$); 108.4 (Cq); 123.6 (CH); 127.2 (CH); 127.8 (CH); 128.4 (CH); 128.8 (CH); 129.2 (CH); 129.6 (CH); 129.8 (CH); 130.2 (CH); 130.3 (CH); 132.1 (Cq); 134.3 (Cq); 135.7 (Cq); 138.2 (Cq); 144.0 (CH); 150.0 (Cq); 152.6 (Cq); 157.2 (Cq).

COMPOUND 25c

^{1}H-NMR (600 MHz, CD$_3$CN, +25 °C): δ 3.56 (s, CH$_3$); 5.46 (s, CH$_2$); 7.31-7.38 (m, 5H); 7.45 (d, *J*=7.4 Hz, 1H); 7.49-7.51 (m, 1H); 7.55-7.58 (m, 1H); 7.61-7.63 (m, 1H); 7.66 (d, *J*=8.2 Hz, 1H); 8.01 (dd, *J*=8.2, 2.4 Hz, 2H).

^{13}C-NMR (150.8 MHz, CD$_3$CN, 1.79 ppm, +25 °C) : δ 30.7 (CH$_3$); 51.1 (CH$_2$); 108.5 (Cq); 123.7 (CH); 127.2 (CH); 127.8 (CH); 128.4 (CH); 128.7 (CH); 129.2 (CH); 129.6 (CH); 129.8 (CH); 130.2 (CH); 130.3 (CH); 132.1 (Cq); 134.8 (Cq); 135.7 (Cq); 138.2 (Cq); 143.7 (CH); 151.7 (Cq); 153.1 (Cq); 156.7 (Cq).

4.5 Kinetic studies

The experimental values of thermal racemization interpolated with the first order reversible kinetic equation of compounds **25b** and **25c** are reported in table 11 and 12.

Table 11 Compound 25b: Racemization process of first eluted enantiomer at T=+30°C, +50°C and +58°C and of second eluted enantiomer at T=+56°C.

T +30 °C		T +50 °C		T +56°C		T +58°C	
t (s)	$\ln(x_{ena1}-x_{ena1\_eq})$	t (s)	$\ln(x_{ena1}-x_{ena1\_eq})$	t (s)	$\ln(x_{ena2}-x_{ena2\_eq})$	t (s)	$\ln(x_{ena1}-x_{ena1\_eq})$
0	-0,90042	0	-0,73397	0	-0,81803	0	-0,90189
74700	-1,59554	2280	-0,95946	1680	-1,09602	3540	-1,48281
97860	-1,81523	5880	-1,25702	5100	-1,77078	7920	-2,29066
-	-	9120	-1,5616	8760	-2,4986	10020	-2,752
-	-	12660	-1,86821	-	-	-	-
-	-	14340	-2,04022	-	-	-	-
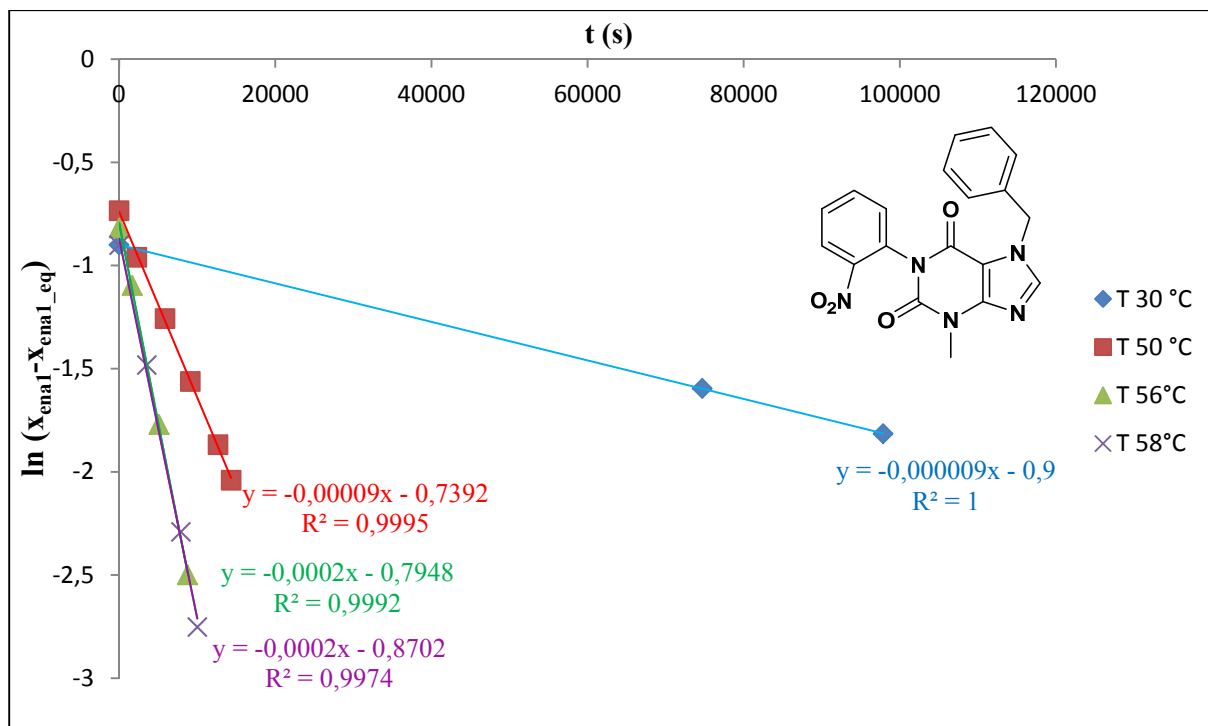
Figure 35 Compound **25b**: Kinetic data fitted with linear regression of first eluted enantiomer at T=+30°C,+50°C and +58°C and of **second eluted** enantiomer at T=+56°C.

Table 12 Compound **25c**: Racemization process at each temperature of second eluted enantiomer

T +100 °C		T +110 °C		T +120 °C		T +130 °C	
t(s)	$\ln(x_{ena2}-x_{ena2-eq})$	t(s)	$\ln(x_{ena2}-x_{ena2-eq})$	t(s)	$\ln(x_{ena2}-x_{ena2-eq})$	t(s)	$\ln(x_{ena2}-x_{ena2-eq})$
0	-0,7529	0	-0,7529	0	-0,7546	0	-0,7546
18720	-0,77653	13860	-0,80386	3900	-0,81622	4860	-0,89575
79200	-0,85637	22980	-0,86917	8460	-0,93777	9960	-1,07646
93180	-0,87156	-	-	11940	-1,00731	13080	-1,19733
-	-	-	-	14340	-1,05354	16800	-1,3356
-	-	-	-	66960	-1,7043	21360	-1,50328
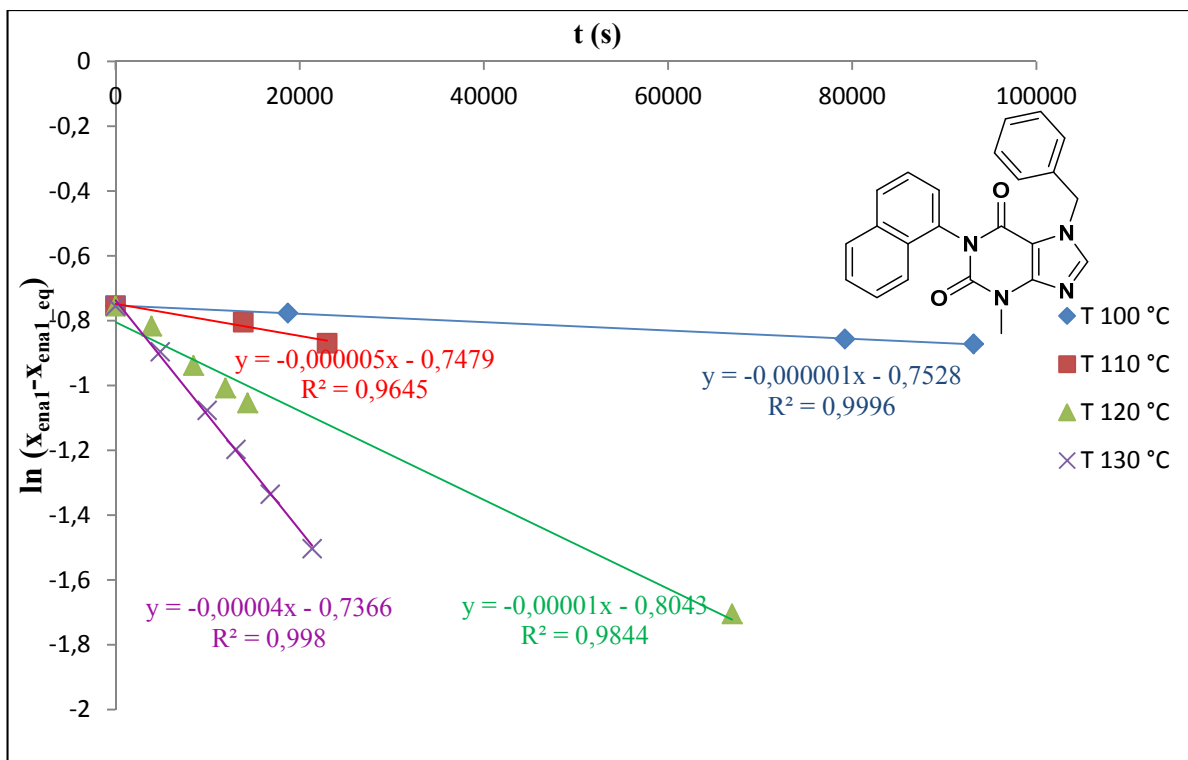
Figure 36 Compound 25c: Kinetic data of second eluted enantiomer fitted with linear regression

The chart contains the following regression equations:

$y = -0{,}000005x - 0{,}7479$
$R^2 = 0{,}9645$

$y = -0{,}000001x - 0{,}7528$
$R^2 = 0{,}9996$

$y = -0{,}00004x - 0{,}7366$
$R^2 = 0{,}998$

$y = -0{,}00001x - 0{,}8043$
$R^2 = 0{,}9844$

Axis label (y): $\ln\left(x_{ena1} - x_{ena1\_eq}\right)$

Axis label (x): t (s)

Legend: T 100 °C, T 110 °C, T 120 °C, T 130 °C

4.6 Absolute configuration

As addressed in *Result and discussion* the calculated and experimental ECD spectra of compound **25b** are reported below.

UV/Vis spectrum
Compound 25b

Experimental ECD spectrum
Second eluted enantiomer

Figure 37 Experimental UV/Vis and ECD spectra of compound 25b

Figure 38 Compound 25b: Calculated and experimental ECD spectra the second eluted enantiomer has absolute configuration M

5. Appendix

5.1 Density Functional Theory (DFT)

Up to the end of the 1990s, conformational calculations of organic molecules were mainly performed by molecular mechanics (e.g., MM3,[56] MMX,[57] MMFF,[58] Amber[59] etc.) and semiempirical methods (AM1,[60] PM3,[61] MINDO[62] being the most popular).

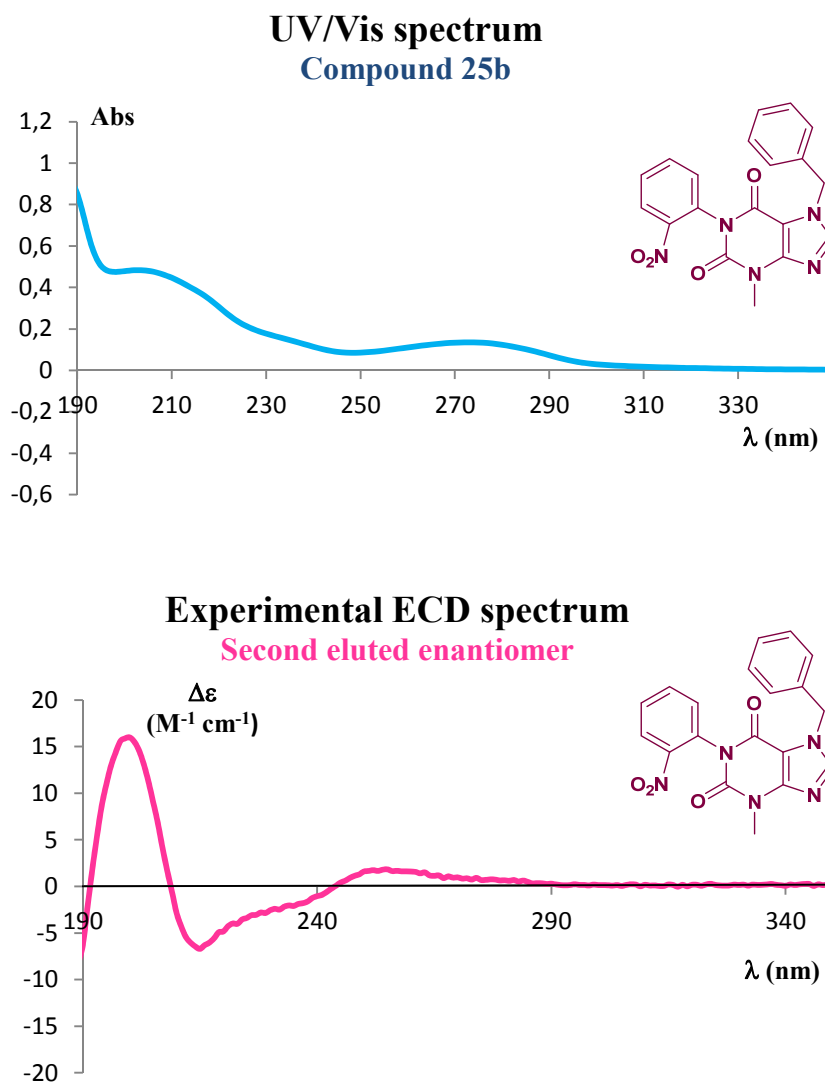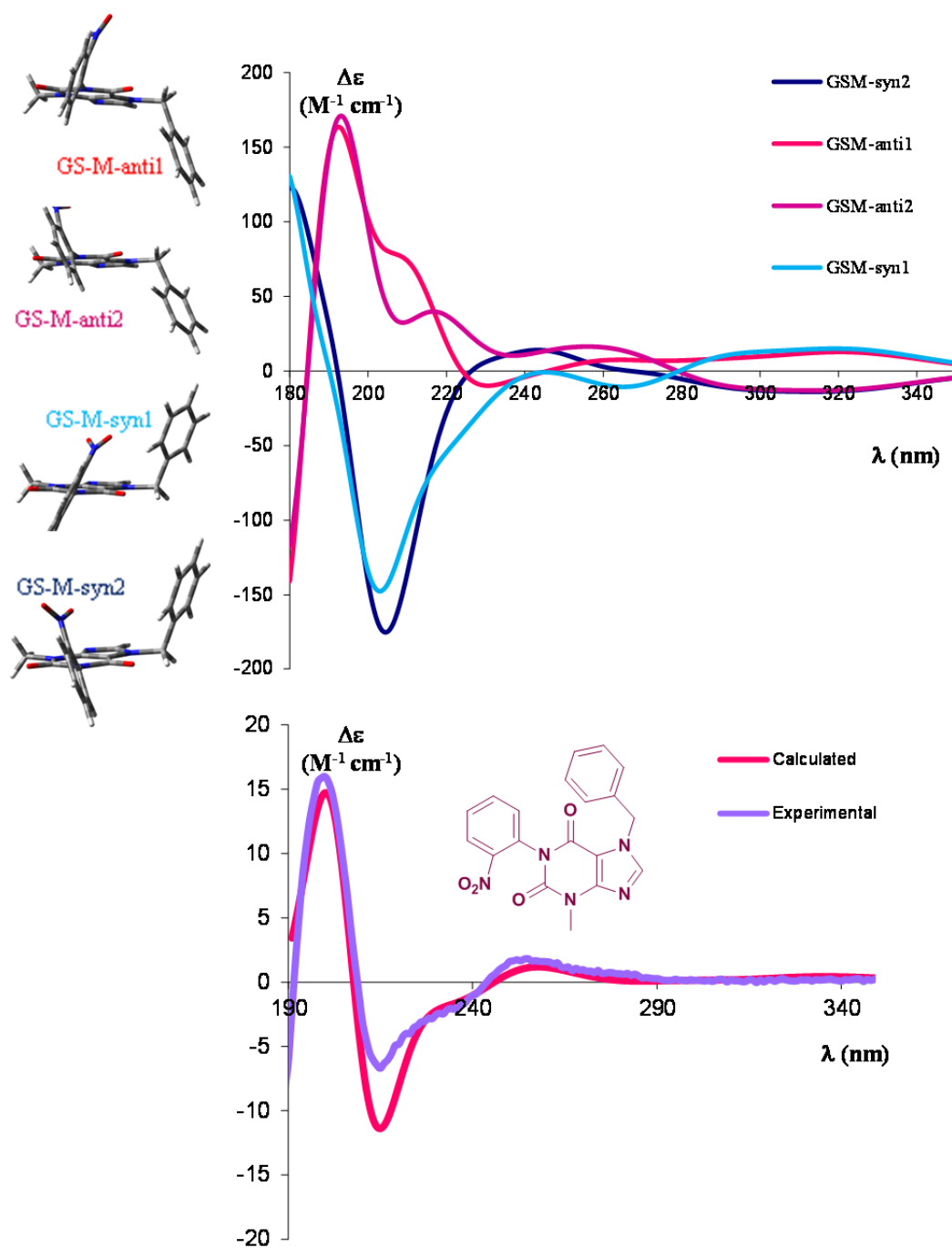The results obtained were often quite accurate, at least for the calculation of the ground-state conformations. For the calculation of transition states, in contrast, these methods have intrinsic limitations. Usually the interconversion barriers were calculated by moving the relative parts of the molecule in fixed steps and optimizing the remaining parts. Otherwise, a "handmade" transition state was assumed, and the geometry was optimised within certain constraints. As a result of these approximations, the computed barriers were prone to relatively large errors, and there was no guarantee that a real transition state had been located.[63]

When the application of *ab initio* methods (HF) became available for medium-sized molecules the situation was greatly improved, although the neglecting of electron correlation was a serious limitation, partially solvable only through the employment of higher methods such as MP2.[64] Unfortunately, this approach was not manageable without a very large computational facility.

On the contrary, Density Functional Theory (DFT) has the great advantage of taking account of electronic correlation at a reasonable computational cost.[65] The basic idea of DFT is that for a collection of electrons and nuclei the ground state molecular energy, the wavefunction and all other molecular electronic properties are uniquely determined by the electron probability density $\rho(x,y,z)$, a function of three variables. The ground state energy, E_0, is a functional of ρ: $E_0 = F[\rho]$.[66]

In recent years, the availability of inexpensive high-performance servers and manageable software (Gaussian 09,[53] and Spartan being the most famous) has allowed high-level calculations to be performed in a reasonable amount of time for molecules containing up to 50–60 atoms.

DFT calculations are very interesting because they can be applied both to obtain the conformations of ground states and also to find the correct geometries and energies of ground and transition states. Thanks to vibrational analysis, there is always confirmation that the correct transition state has been unambiguously identified.

Ground states

Some uncertainty is involved in determining the relative energies of possible ground states. In recent years many papers addressing the performance of various DFT functionals in determining relative energies in reactions have appeared,[67] but for conformational analysis there have been very few.

For accuracy consideration the smallest basis set used is generally 6-31G* or the equivalent. Interestingly, there is only a small increase in accuracy obtained by using very large basis sets. This is probably due to the fact that the density functional has limited accuracy compared to that of the basis set. The accuracy of results from DFT calculations can be poor to fairly good, depending on the choice of basis set and density functional.

The geometries obtained by calculations can in many cases be checked by X-ray diffraction data, and the relative energies of conformations can be compared with the results of kinetic studies. Although such a calculation usually refers to an isolated molecule, whereas X-ray studies reflect the solid state and kinetic results are for solutions, DFT structures compare very well with experimental observations in almost all cases, and the relative energies of possible conformations are correctly calculated.

Transition states

The determination of transition state structures and energies is a crucial point for dynamic analysis, because the correct simulation of energy barriers could greatly help the understanding of dynamic processes. As addressed by D. Young,[68] a transition state (or saddle point) structure is mathematically defined as "*the geometry that has zero derivative of energy with respect to moving every one of the nuclei, and has positive second derivative energy for all but one geometric movement*". In other words, a transition state linking two energy minima represents a maximum of energy in the direction of the reaction path, but it is a minimum in all other directions.

Once a stationary point is found, the primary way to verify whether it corresponds to a transition state is to compute the vibrational frequencies. A transition state must have only one negative (i.e., imaginary) frequency, and the vibrational motion associated with this frequency corresponds to the motion going towards reagents in one direction, and towards the products in the other.

Unfortunately, in contrast with the transition states for high-energy processes (such as those involved in a chemical reaction), in which the imaginary frequency usually has a large (negative) value, the transition states involved in internal dynamic processes usually display small negative vibrational frequencies and can therefore be difficult to locate, especially in the presence of other possible internal motions. On the other hand, the geometry of a transition state is much simpler to idealise, because many geometrical parameters are fixed by the molecular scaffold.

5.2 Electronic Circular Dichroism (ECD)

The knowledge of absolute configuration is mandatory in many industrial applications. For pharmaceutical applications, it is required that the absolute configuration of chiral drugs is known and that the biological activity of the compounds is tested for both enantiomers. Production of new drugs also requires a verification of the enantiomeric purity of the compounds. This leads to the need for characterizing their chiral purity and absolute configuration. One widely used method to detect and analyse chirality is the determination of the optical activity by circular dichroism (CD).[69] In biology, for example, electronic circular dichroism (ECD) spectra are frequently used to characterize the secondary structure of proteins. [70]

Circular dichroism (CD) is the difference in the absorption of left-handed circularly polarized light (L-CPL) and right-handed circularly polarized light (R-CPL) and occurs when a molecule contains one or more chiral chromophores (light-absorbing groups). Measurements carried out in the visible and ultra-violet region of the electro-magnetic spectrum monitor electronic transitions, and, if the molecule under study contains chiral chromophores then one CPL state will be absorbed to a greater extent than the other and the CD signal over the corresponding wavelengths will be non-zero. A circular dichroism signal can be positive or negative, depending on whether L-CPL is absorbed to a greater extent than R- CPL (positive CD signal) or to a lesser extent (negative CD signal).

Linearly polarized light is light whose oscillations are confined to a single plane. All polarized light states can be described as a sum of two linearly polarized states at right angles to each other, usually referenced to the viewer as vertically and horizontally polarized light.
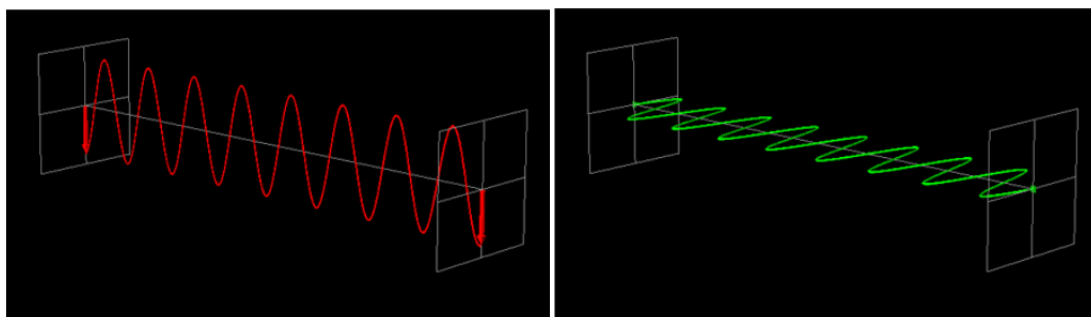

Figure 39 Vertically and horizontally Polarized Light

If for instance we take horizontally and vertically polarized light waves of equal amplitude that are in phase with each other, the resultant light wave (blue) is linearly polarized at 45 degrees.
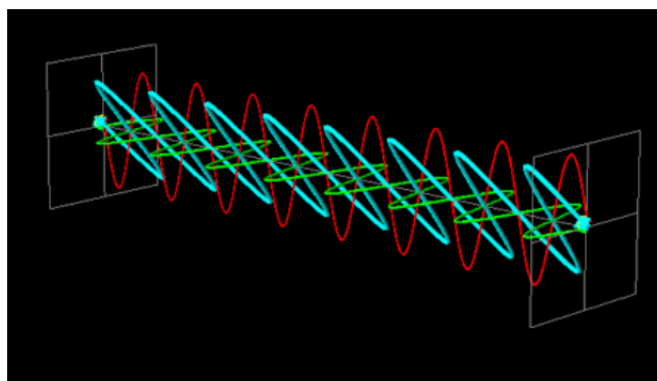

Figure 40 45° Polarized Light

If the two polarization states are out of phase, the resultant wave ceases to be linearly polarized. For example, if one of the polarized states is out of phase with the other by a quarter-wave, the resultant will be a helix and is known as circularly polarized light (CPL). The helices can be either right-handed (R-CPL) or left-handed (L-CPL) and are non-superimposable mirror images.
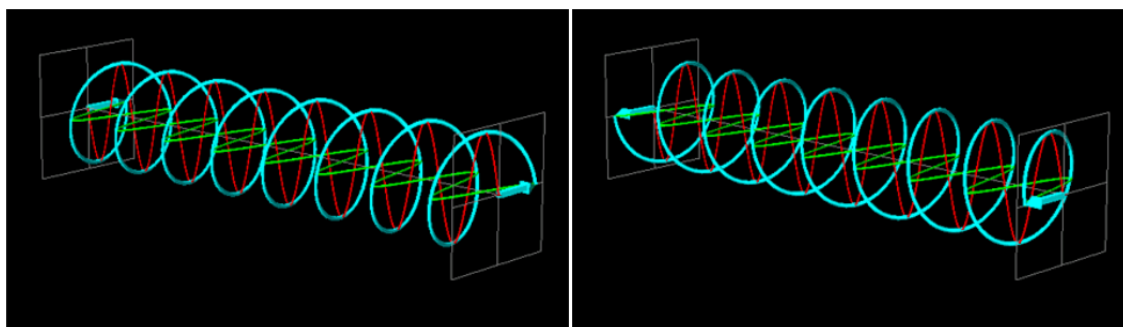
Figure 41 Left Circularly Polarised (LCP) Light Right Circularly Polarised (RCP) Light

The difference in absorbance of left-hand and right-hand circularly polarized light is the basis of circular dichroism. A molecule that absorbs LCP and RCP differently is *optically active*, or *chiral*. In fact, whenever a circularly polarized radiation flows through a medium with chiral properties, acquires elliptical polarization, whose plane undergoes a rotation. The elliptical polarization occurs because the dextrorotatory (E_R) and levorotatory (E_L) components of the electric field vector, constituting the electromagnetic wave, are differently absorbed by an

optically active substance: therefore it is necessary to introduce two absorptivity, ε_R and ε_L, one for each of the two vector components.[69,71]

$$\Delta\varepsilon = \varepsilon_L - \varepsilon_R$$

The rotation of plane is due to the different refractive indices, n_R and n_L, generated from the interaction between the component E_R and E_L respectively, and the chiral substance. The result is that the vector components don't propagate with the same speed but one is more accelerated respect the other.

It is possible to predict the ellipticity (ψ) and the angle (α) of rotation of the plane of a polarized radiation, after its interaction with an optically active medium, by means of the following equations:

$$\psi = (\varepsilon_L\text{-}\varepsilon_R)\,\frac{\pi\,l}{\lambda} \qquad\qquad \alpha = (n_L\text{-}n_R)\frac{\pi\,l}{\lambda}$$

where λ is the wavelength of the monochromatic polarized radiation, and l is the path length through the medium chiral . The values of ψ and α are expressed in radians.
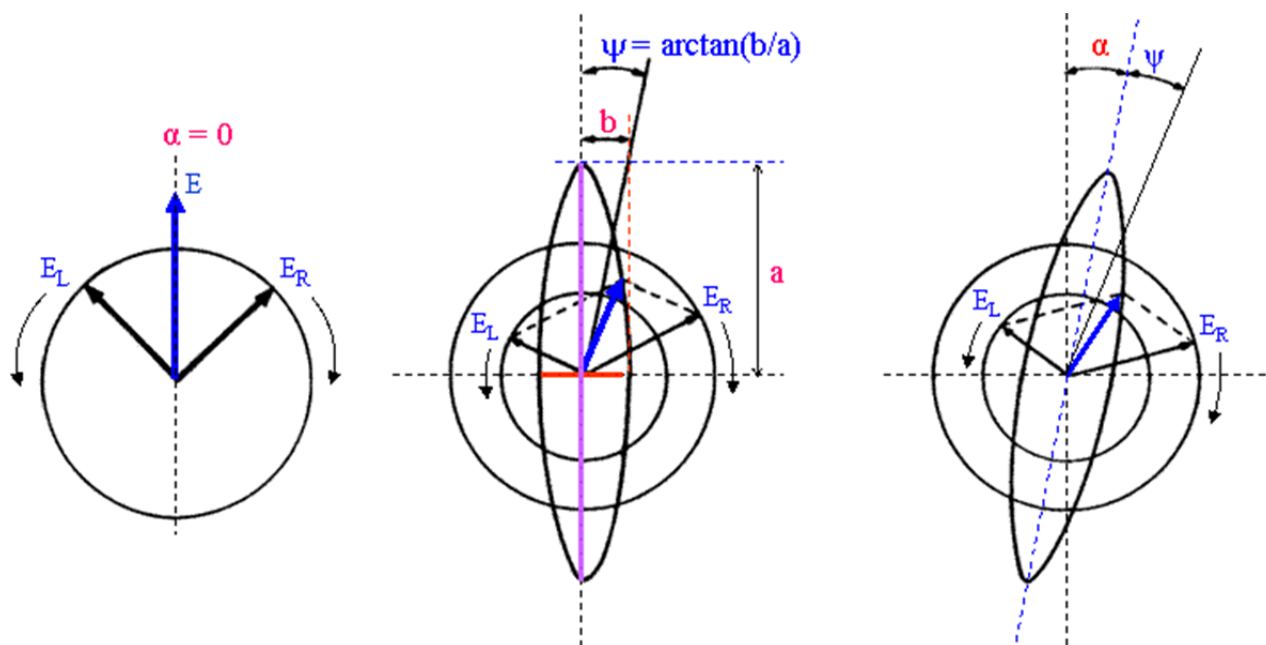

Figure 42 Ellipticity and rotation of the plane of a polarized radiation

CD may be regarded as one of the most powerful techniques for stereochemical analyses: it is sensitive to the absolute configuration as well as to conformational features, which are often completely obscured in the ordinary absorption spectrum.[72]

The CD of pure enantiomers differs in sign, but not in magnitude. Unfortunately, there is no simple relationship between the absolute configuration of an enantiomer and the sign of its ECD spectrum: CD depends on details of the electronic and geometric molecular structure.[73]

The experimental CD of the molecule under investigation is commonly displayed together with either another experimental spectrum, or with the result of a more or less sophisticated calculated theoretical curve; in both cases it is very important to correctly choose the reference data. An example of experimental and calculated comparison is reported in figure 43.
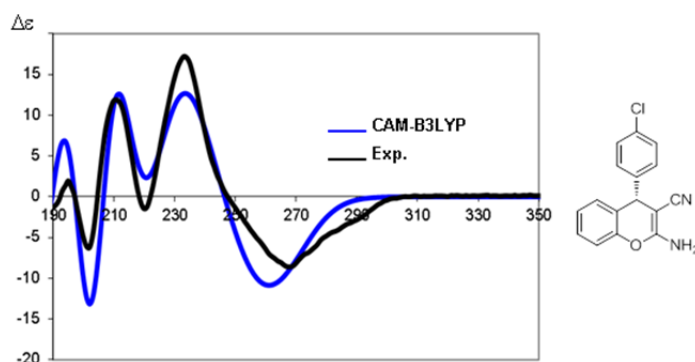

Figure 43 Calculated CAM-B3LYP (blue line) and experimental (black line) ECD spectrum of the (*S*)-2-Amino-4-(4-chlorophenyl)-6-methyl-4*H*-chromene-3-carbonitrile [74]

The spectra of two enantiomers of a chiral molecule are conditioned by the chromophores in their environment. Every conformational difference, every major alteration in the nature of the chromophore or of the perturbing groups between the test and reference makes the comparison and determination of absolute configuration unreliable. The appearance of the CD spectrum, namely position, intensity and sign of the bands, reflects the environment of each chromophore.

ECD and optical rotation depend sensitively on the presence and nature of solvent interactions.[75] The change in chiroptical response due to solute–solvent interactions is sometimes drastic and non-intuitive. A well-known example is the sign inversion in the optical rotation of methyloxirane upon changing the solvent from water to benzene.[76]

Classical force-field MD simulations constitute a possible route to explicitly account for interactions between molecule and solvent.[77] Apart from the high computational cost it might appear most desirable to treat the solute embedded in a large number of solvent molecules within a first-principles quantum mechanical MD approach. This might only be possible with very efficient electronic structure methods such as DFT which on the other hand have

deficiencies for non-covalent long-range interactions.[78] Time-dependent density functional theory (TD-DFT) is presently the most widely used electronic structure method for ECD calculations. It extends the basic ideas of ground-state density-functional theory (DFT) to the treatment of excitations or more general time-dependent phenomena.

It turns out that, even with the simplest approximation to the Kohn-Sham potential, spectra calculated within this framework are in very good agreement with experimental results.[79]

References

[1] Wolf, C. *Dynamic Stereochemistry of Chiral Compounds*, **2008**.

[2] Bringmann, G.; Price Mortimer, A. J.; Keller, P. A.; Gresser, M. J.; Garner, J.; Breuning, M. *Angew. Chem. Int. Ed.* **2005**, *44*, 5384.

[3] Kuhn, R.; Freudenberg, K. Ed.; Deuticke, F.; *"Molekulare asymmetrie", Stereochemie* **1933**, *803*.

[4] Aitken, R. A.; Kilenyi, S. N. *Asymmetric Synthesis* **1994**, *15*.

[5] Christie, H.G.; Kenner, J. H. *J. Chem. Soc.* **1922**, *121*, 614..

[6] Oki, M. *Topics in Stereochemistry* **1983**.

[7] Compendium of Chemical Terminology, Goldbook- International Union of Pure and Applied Chemistry, version 2.3.1 2012.

[8] *a)* Clayden, J.; Moran, W. J.; Edwards, P. J.; LaPlante, S. R. *Angew. Chem. Int. Ed.* **2009**, *48*, 6398–6401. *b)* LaPlante, S. R.; Fader, L. D.; Fandrick, K. R.; Fandrick, D. R.; Hucke, O.; Kemper, R.; Miller, S. P. F.; Edwards, P. J. *J. Med. Chem.* **2011**, *54*, 7005–7022. *c)* LaPlante, S. R.; Edwards, P. J.; Fader, L. D.; Jakalian, A.; Hucke, O. *ChemMedChem* **2011**, *6*, 505–513.

[9] Noyori, R.; Tkaya, H. *Acc. Chem. Res.* **1990**, *23*, 345–350

[10] *a)* Blaschke, G.; Kraft, H. P.; Fickentscher, K.; Köhler, F. *Arzneim.-Forsch.* **1979**, *29*, 1640–1642; *b)* Fabro, S.; Smith, R. L.; Williams, R. T.; *Nature* **1967**, *215*, 296–297; *c)* Reist, M.; Carrupt, P.-A.; Francotte, E.; Testa, B. *Chem. Res. Toxicol.* **1998**, *11*, 1521–1528; *d)* Eriksson, T.; Bjorkman, S.; Roth, B.; Fyge, A.; Hoglund, P. *Chirality* **1995**, *7*, 44–52.

[11] Agranat, I.; Caner, H.; Caldwell, J. *Nat. Rev. Drug Discovery* **2002**, *1*, 753–768; *b)* Rouhi, A. M. *Chem. Eng. News* **2003**, *81*, 18, 56–61.

[12] a) Department of Health & Human Services, Food and Drug administration: FDA_sPolicy Statement for the Development of New Stereoisomeric Drugs, Washington, C, **1992**: *http://www.fda.gov/Drugs/GuidanceComplianceRegulatoryInformation/Guidances/ucm*; b) Miller, S. 18th International Symposium on Chirality, Busan, Korea, June 26, **2006**: *www.fda.gov/downloads/AboutFDA/CentersOffices/CDER/ucm103532.pd*.

[13] Chen, C. S.; Shieh, W. R.; Lu, P. H.; Harriman, S.; Chen, C. Y. *Biochim. Biophys. Acta Protein Struct. Mol. Enzymol.* **1991**, *1078*, 411–417; b) Tracy, T. S.; Hall, S. D.; *Drug Metab. Dispos.* **1992**, *20*, 322–327.

[14] Eveleigh, P.; Hulme, E. C.; Schudt, C.; Birdsall, N. J. M. *Mol. Pharmacol.* **1989**, *35*, 477–483.

[15] *a)* Tucci, F. C.; Hu, T.; Mesleh, M. F.; Bokser, A.; Allsopp, E.; Gross, T. D.; Guo, Z.; Zhu, Y.-F.; Struthers, R. S.; Ling, N.; Chen, C. *Chirality* **2005**,*17*, 559 – 564.

[16] Friary, R. F.; Spangler, M.; Osterman, R.; Schulman, L.; Schwerdt, J. H. *Chirality* **1996**, *8,* 364–371.

[17] *a)* Betson, M. S.; Clayden, J.; Worrall, C. P.; Peace, S. *Angew. Chem. Int. Ed.* **2006**, *45*, 5803; *b)* Adler, T.; Bonjoch, J.; Clayden, J.; Font-Bardfa, M.; Pickworth, M.; Solans, X.; Sole, D.; Vallverdu, L. *Org. Biomol. Chem.* **2005**, *3*, 3173; *c)* Curran, D. P.; Qi, H.; Geib, S. J.; DeMello, N. C. *J. Am. Chem. Soc.* **1994**, *116*, 3131; d*)* Clayden, J. P.; Lai, L. W. *Angew. Chem. Int. Ed.* **1999**, *38*, 2556. *e)* Cuyegkeng, M. A.; Mannschreck, A. *Chem. Ber.* **1987**, *120*, 803; *f)* Pinkus, A. G.; Riggs, J. I.; Broughton, S. M. *J. Am. Chem. Soc.* **1968**, *90*, 5043; *g)* Michalik, J. *Chem. Soc. Perkin Trans. 2* **2002**, *114*; *h)* Lam, W. Y.; Martin, J. C. *J. Org. Chem.* **1981**, *46*, 4458; *i)* Furusho, Y.; Aida, T.; Inoue, S. *Chem. Commun.* **1994**, *653*.

[18] Mino,T.;Tanaka,Y.;Yabusaki,T.; Okumura,D.; Sakamoto,M.;Fujiita,T. *Tetrahedron: Asymm.* 2003, 14, 2503-2506.

[19] Casarini D.; Foresti, E., Lunazzi, L.; Macciantelli, D. *J.Am. Chem. Soc.* **1988**, *110*, 4527-4532.

[20] Garcia, M.; Grilli, S.; Lunazzi, L.; Mazzanti, A.; Orelli L. R. *J.Org.Chem.* **2001**, *66*, 6679-6684.

[21] Curran, D.; Qi, H.; Geib, S.; DeMello, N.C. *J.Am.Chem.Soc.***1994**, *116*, 3131-3132

[22] Haushalter, K.; Lau, J.; Roberts, J.D. *J. Am. Chem.Soc.* **1996**,*118*,8891-8896.

[23] Oguz, S.F.; Dogan*,* I. *Tetrahedron: Asymm.* **2003**, *14*, 1857-1864.

[24] Carey, A. F.; Sundberg, R. Advanced Organic Chemistry, Part A:Structure and Mechanism; Plenum Press: New York, **1990**, 120.

[25] Zask, A.; Murphy, J.; Ellestad, G.A. *Chirality*, **2013**, *25*, 265–274.

[26]*https://en.wikipedia.org/wiki/Stimulant*

[27] *https://en.wikipedia.org/wiki/Caffeine*

[28] *https://en.wikipedia.org/wiki/Theobromine*

[29] *https://en.wikipedia.org/wiki/Hypoxanthine*

[30] *https://en.wikipedia.org/wiki/Xanthine_oxidase*

[31] *https://en.wikipedia.org/wiki/Purine_nucleoside_phosphorylase*

[32] Voet, D.; Voet, J.; Pratt, C. *Fundamentals of Biochemistry: Life at the Molecular Level*, **2008**, 840.

[33] Yu, M.; Wang,J.; Mura, M.; Meng, Q.; Xu, W.; Gersen, H.; Lægsgaard, H.; Stensgaard, I.; Kelly, R. E. A.; Kjems, J.; Linderoth, T. R.; Kantorovich, L. N.; Besenbacher, F. *Acsnano* **2011**, *5*, (8), 6651−6660.

[34] He, R.; Lam, Y. *J. Comb. Chem.* **2005**, *7,* 916-920.

[35] Ciesielski, A.; Haar, S.; Bényei, A.; Paragi, G.; Guerra, C. F.; Bickelhaupt, F. M.; Masiero, S.; Szolomájer, J.; Samorì, P.; Spada, G. P.; Kovács, L. *Langmuir* **2013**, *29*, 7283−7290.

[36] *https://en.wikipedia.org/wiki/Sympathomimetic_drug*

[37] *https://en.wikipedia.org/wiki/Adenosine*

[38] *https://en.wikipedia.org/wiki/Central_nervous_system*

[39] Schneller, S. W.; Ibay, C.; Christ, W. J.; Brunst, R. F. *J. Med. Chem.* **1989**, *32*, 2254-2260.

[40] Mder, E.; Shi, D.; Manning, M.; Daly, J. W. *J. Med. Chem.* **1993***,36,* 3341-3349.

[41] Lyles, M. B.; Cameron, I. L.; Rawls, H. R. *Journal of Medicinal Chemistry*, **2001**, *44*, 4657.

[42] LaPlante,S. R.; Fader,L. D.; Fandrick,K. R.; Fandrick,D. R.; Hucke,O.; Kemper,R.; Miller,S. P. F.; Edwards, P. J.*J. Med. Chem.***2011**, 54, 7005–7022.

[43] a) Bridson, P. K.; Wang, X. *Synthesis,* **1995**, 855-858; b) He, R.;. Lam, Y *J. Comb. Chem.* **2005**, *7*, 916-920; c) Zavialov, I. A.; Dahanukar, V. H.; Nguyen, H.; Orr, C.; Andrews D. R. *Organic Letters* **2004**, *6*, 2237-2240.

[44] L. Lunazzi, M. Mancinelli, A. Mazzanti, S. Lepri, R. Ruzziconi, M. Schlosser *Org. Biomol. Chem.* **2012**, *10*, 1847-1855.

[45] Eyring, H. *Chem. Revs.* **1935**, 17, 65 − 77.

[46] Casarini, D.; Lunazzi, L.; Mazzanti, A. *Eur. J. Org. Chem.* **2010**, 2035- 2056.

[47] Berova, N.; Di Bari, L.; Pescitelli, G. *Chem. Soc. Rev.* **2007**, *36*, 914–931.

[48] Yanai, T.; Tew, D.; Handy, N. *Chem. Phys. Lett.* **2004**, *393*, 51−57.

[49] a) Ambrogi, M.; Ciogli, A.; Mancinelli, M.; Ranieri, S.; Mazzanti, A. *J. Org. Chem.*, **2013**, *78,* 3709–3719; b) Gunasekaran, P.; Perumal, S.; Menéndez, J.C.; Mancinelli, M.; Ranieri, S.; Mazzanti, A. *J. Org. Chem.*, **2014**, *79*, 11039–11050.

[50] Michl, J.; Thulsturp, E. W. *Spectroscopy with Polarized Light*; VCH Publisher Inc.: New York, 1986.

[51] Tinnis, F.; Stridfeldt, E.; Lundberg, H.; Adolfsson, H.; Olofsson, B. *Org. Lett.* **2015**, *17,* 2688.

[52] ComputeVOA 0.1: Software package for conformational calculation, integrated with Gaussian09. *www.btools.com/products.html/#software*.

[53] Gaussian 09, rev D.01. Frisch, M. J.; Trucks, G. W.; Schlegel, H. B.; Scuseria, G. E.; Robb, M. A.; Cheeseman, J. R.; Scalmani, G.; Barone, V.; Mennucci, B.; Petersson, G. A.; Nakatsuji, H.; Caricato, M.; Li, X.; Hratchian, H. P.; Izmaylov, A. F.; Bloino, J.; Zheng, G.; Sonnenberg, J. L.; Hada, M.; Ehara, M.; Toyota, K.; Fukuda, R.; Hasegawa, J.; Ishida, M.; Nakajima, T.; Honda, Y.; Kitao, O.; Nakai, H.; Vreven, T.; Montgomery, Jr., J. A.; Peralta, J. E.; Ogliaro, F.; Bearpark, M.; Heyd, J. J.; Brothers, E.; Kudin, K. N.; Staroverov, V. N.; Kobayashi, R.; Normand, J.; Raghavachari, K.; Rendell, A.; Burant, J. C.; Iyengar, S. S.; Tomasi, J.; Cossi, M.; Rega, N.; Millam, N. J.; Klene, M.; Knox, J. E.; Cross, J. B.; Bakken, V.; Adamo, C.; Jaramillo, J.; Gomperts, R.; Stratmann, R. E.; Yazyev, O.; Austin, A. J.; Cammi, R.; Pomelli, C.; Ochterski, J. W.; Martin, R. L.; Morokuma, K.; Zakrzewski, V. G.; Voth, G. A.; Salvador, P.; Dannenberg, J. J.; Dapprich, S.; Daniels, A. D.; Farkas, O.; Foresman, J. B.; Ortiz, J. V.; Cioslowski, J.; Fox, D. J. Gaussian, Inc., Wallingford CT, **2009**.

[54] Package GaussView 5.0.9, Gaussian Inc., Wallingford CT, **2009**.

[55] a) Bridson, P. K.; Wang, X. *Synthesis,* **1995**, 855-858; b) He, R.;. Lam, Y *J. Comb. Chem.* **2005**, *7*, 916-920; c) Zavialov, I. A.; Dahanukar, V. H.; Nguyen, H.; Orr, C.; Andrews D. R. *Organic Letters* **2004**, *6*, 2237-2240.

[56] Allinger, N. L.; Yuh, Y. H.; Lii, J.-H. *J. Am. Chem. Soc.* **1989**, *111*, 8551–8566.

[57] *PCMODEL*, v9, Serena Software, Bloomington, IN (USA).

[58] Halgren, T. A. *J. Comput. Chem.* **1996**, *17*, 520–552.

[59] Weiner, S. J.; Kollman, P. A.; Case, D. A.; Singh, U. C.; Ghio, C.; Alagona, G.; Profeta, S.; Weiner, P. *J. Am. Chem. Soc.* **1984**, *106*, 765–784.

[60] Dewar, M. J. S.; Zoebisch, E. G.; Healy, E. F.; Stewart, J. J. P. *J. Am. Chem. Soc.* **1985**, *107*, 3902–3909.

[61] Stewart, J. J. P. *J. Comput. Chem.* **1989**, *10*, 209–220; Stewart, J. J. P. *J. Comput. Chem.* **1989**, *10*, 221–264.

[62] Bingham, R. C.; Dewar, M. J. S.; Lo, D. H. *J. Am. Chem. Soc.* **1975**, *97*, 1285–1293

[63] Casarini, D.; Lunazzi, L.; Mazzanti, A. *Eur. J. Org. Chem.* **2010**, 2035- 2056.

[64] Frisch, M. J.; Head-Gordon, M.; Pople, J. A. *Chem. Phys. Lett.* **1990**, *166*, 281–289.

[65] Koch, W.; Holthausen, M. C. *A Chemist's Guide to Density Functional Theory*, Wiley-VCH, Weinheim, 2nd ed., **2002**; *A Primer in Density Functional Theory* (Eds.: Fiolhais, C.; Nogueira, F.; Marques, M.), Springer-Verlag, Heidelberg, **2003**.

[66] Mitchell, P. C. H. *Appl. Organometal. Chem.* **2000**, *14*, 744–747 in the preface to: *A Chemist's Guide to Density Functional Theory* Koch, W.; Holthausen, M. C. Wiley-VCH, Weinheim, 2nd ed., **2002**.

[67] a) Check, C. E.; Gilbert, T. M. *J. Org. Chem.* **2005**, *70*, 9828– 9834; b) Wodrich, M. D.; Corminbouef, C.; Schleyer, P. v. R. *Org. Lett.* **2006**, *8*, 3631–3634; c) Shreiner, P. R.; Fokin, A. A.; Pascal, R. A.; De Mejere, A. *Org. Lett.* **2006**, *8*, 3635–3638; d) Grimme, S. *Angew. Chem. Int. Ed.* **2006**, *45*, 4460–4464; e) Zhao, Y.; Truhlar, D. G. *Org. Lett.* **2006**, *8*, 5753– 5755; f) Rokob, T. A.; Hamza, A.; Pápai, I. *Org. Lett.* **2007**, *9*, 4279–4282; g) Shreiner, P. R. *Angew. Chem. Int. Ed.* **2007**, *46*, 4217–4219; h) Wodrich, M. D.; Wannere, C. S.; Mo, Y.; Jarowski, P. D.; Houk, K. N.; Schleyer, P. v. R. *Chem. Eur. J.* **2007**, *13*, 7731–7744; i) Zhao, Y.; Truhlar, D. G. *Acc. Chem. Res.* **2008**, *41*, 157–167; j) Schwabe, T.; Grimme, S. *Acc. Chem. Res.* **2008**, *41*, 569–579; k) Wodrich, M. D.; Jana, D. F.; Schleyer, P. v. R.; Corminbouef, C. *J. Phys. Chem. A* **2008**, *112*, 11495–11500.

[68] Young, D. *Computational Chemistry*, chapter 17, pp. 147– 158, Wiley Interscience, New York, **2001**.

[69] Berova, N.; Nakanishi, K.; Woody, R. W. *Circular dichroism, Principles and applications*, 2nd Edition, Wiley-VCH, **2000**.

[70] a) Fasman GD. *Circular Dichroism and the Conformational Analysis of Biomolecules*. New York: Plenum Press; **1996**. b) Manavalan, P; Johnson, W.C. *J Biosci* **1985**, *8*, 141–149. c) Sreerama, N; Venyaminov, SY; Woody, RW. *Anal Biochem* **2000**, *287*, 243–251.

[71] Mislow, K. *Introduction to stereochemistry*, **1965**, W. A. Benjamin, Inc.

[72] Berova, N.; Di Bari, L.; Pescitelli, G. *Chem. Soc. Rev.* **2007**, *36*, 914–931.

[73] *WIREs Comput Mol Sci* **2012**, *2,* 150–166.

[74] Caruana, L.; Mondatori, M.; Corti, V.; Morales, S.; Mazzanti, A.; Fochi, M. Bernardi, L. *Chem. Eur. J.* **2015**, 21, 6037-6041.

[75] a) Kongsted, J.; Pedersen, T. B.; Osted, A.; Hansen, A. E.; Mikkelsen, K. V.; Christiansen, O. *J. Chem. Phys. A* **2004**, *108*, 3632–3641. b) Müller, T.; Wiberg, K. B.; Vaccaro, P. H. *J. Chem. Phys. A* **2000**, *104*, 5959–5968. c) Kumata, Y.; Furukawa, J.; Fueno, T. *Bull. Chem. Soc. Jpn.* **1970**, *43*, 3920–3921. d) Mukhopadhyay, P.; Zuber, G.; Goldsmith, M.; Wipf, P.; Beratan, D. N. *Chem. Phys. Chem.* **2006**, *7*, 2483–2486.

[76] Kumata Y, Furukawa J, Fueno T. *Bull. Chem. Soc. Jpn.* **1970**, *43*, 3920–3921.

[77] a) Kundrat, M. D.; Autschbach, J. *J. Chem. Theory Comput.* **2009**, *5*, 1051–1060. b) Mukhopadhyay, P.; Zuber, G.; Goldsmith, M.; Wipf, P.; Beratan, D.N. *Chem. Phys. Chem.*

2006, *7*, 2483–2486. c) Bernasconi, L.; Blumberger, J.; Sprik, M.; Vuilleumier, R. *J. Chem. Phys.* **2004**, *121*, 11885–11899.

[78] Autschbach, J. *Chirality* **2009**, *21*, E116– E152.

[79] Marques, M. A. L.; Gross, E. K. U. *Annu. Rev. Phys. Chem.* **2004**, *55*, 427–455.